AN EXPERIMENTAL STUDY ON THE EFFECT OF ULTRASONICATION ON VISCOSITY AND HEAT TRANSFER PERFORMANCE OF AQUEOUS SUSPENSIONS OF MULTI-WALLED CARBON NANOTUBES

A Thesis

by

PARITOSH GARG

Submitted to the Office of Graduate Studies of
Texas A&M University
in partial fulfillment of the requirements for the degree of

MASTER OF SCIENCE

May 2008

Major Subject: Mechanical Engineering

AN EXPERIMENTAL STUDY ON THE EFFECT OF ULTRASONICATION ON VISCOSITY AND HEAT TRANSFER PERFORMANCE OF AQUEOUS SUSPENSIONS OF MULTI-WALLED CARBON NANOTUBES

A Thesis

by

PARITOSH GARG

Submitted to the Office of Graduate Studies of
Texas A&M University
in partial fulfillment of the requirements for the degree of

MASTER OF SCIENCE

Approved by:

Co-Chairs of Committee,	Jorge Alvarado
	Kalyan Annamalai
Committee Members,	Jaime Grunlan
Head of Department,	Dennis O' Neal

May 2008

Major Subject: Mechanical Engineering

ABSTRACT

An Experimental Study on the Effect of Ultrasonication on Viscosity and Heat Transfer Performance of Aqueous Suspensions of Multi-walled Carbon Nanotubes. (May 2008)

Paritosh Garg, B.E., University of Delhi

Co-Chairs of Advisory Committee: Dr. Jorge Alvarado
Dr. Kalyan Annamalai

Through past research, it is known that carbon nanotubes have the potential of enhancing the thermal performance of heat transfer fluids. The research is of importance in electronics cooling, defense, space, transportation applications and any other area where small and highly efficient heat transfer systems are needed. However, most of the past work discusses the experimental results by focusing on the effect of varying concentration of carbon nanotubes (CNTs) on the thermal performance of CNT nanofluids. Not much work has been done on studying the effect of processing variables. In the current experimental work, accurate measurements were carried out in an effort to understand the impact of several key variables on laminar flow convective heat transfer. The impact of ultrasonication energy on CNT nanofluids processing, and the corresponding effects on flow and thermal properties were studied in detail. The properties measured were viscosity, thermal conductivity and the convective heat transfer under laminar conditions. Four samples of 1 wt % multi walled carbon nanotubes (MWCNT) aqueous suspensions with different ultrasonication times were prepared for the study. Direct imaging was done using a newly developed wet-TEM

technique to assess the dispersion characteristics of CNT nanofluid samples. The results obtained were discussed in the context of the CNT nanofluid preparation by ultrasonication and its indirect effect on each of the properties.

It was found that the changes in viscosity and enhancements in thermal conductivity and convective heat transfer are affected by ultrasonication time. The maximum enhancements in thermal conductivity and convective heat transfer were found to be 20 % and 32 %, respectively, in the sample processed for 40 minutes. The thermal conductivity enhancement increased considerably at temperatures greater than 24 $^{\circ}$C. The percentage enhancement in convective heat transfer was found to increase with the axial distance in the heat transfer section. Additionally, the suspensions were found to exhibit a shear thinning behavior, which followed the Power Law viscosity model.

TO MY PARENTS:

FOR THE LOVE, SUPPORT AND ENCOURAGEMENT TO MAKE MY DREAM A REALITY

ACKNOWLEDGEMENTS

I would like to express my sincere gratitude to several people who made this thesis possible. First of all, I would like to thank my co-chair and advisor, Dr. Jorge Alvarado for giving his time and sharing his knowledge on the subject with me. He has always been keen to help me out throughout the course of this research. I would like to thank my other co-chair, Dr. Kalyan Annamalai and my committee member,Dr. Jaime Grunlan for their valuable input.

Additionally, I want to thank Dr. Charles Marsh and his other team members from US Army Corps of Engineers, Engineer Research and Development (ERDC) in Champaign, Illinois for their kind support in sharing their knowledge in the nanofluid research and in imaging the carbon nanotube nanofluids using wet-TEM. I also thank my other research team members: Guillermo Soriano, Landon Jay Sommer, Benjamin Baker and Daniel Escatel for helping in the experimental work.

In closing, I want to thank my parents, Mr. Naresh Kumar Garg and Mrs. Krishna Garg, and my other family members, for encouraging me to pursue higher education. My family members have been the pillars of support in difficult times and always believed in my capabilities.

NOMENCLATURE

K	Flow consistency index
n	Flow behavior index
R_c	Radius of the sample container
R_{sp}	Radius of the spindle
N	Rotational speed of the spindle
M	Torque input by the viscometer
L	Effective length of the spindle
$\dot{q}$	Rate of heat dissipation
k	Thermal conductivity of the medium
Ei	Exponential integral
t	Time
t_1	Heating time
r	Radial distance from the heating source
x	Axial distance from the inlet of the test section
$h(x)$	Convective heat transfer coefficient at a distance, x from the inlet
$q_s^{"}$	Heat flux applied to the fluid
$T_s(x)$	Surface or wall temperature at a distance, x from the inlet
$T_b(x)$	Fluid bulk temperature at a distance, x from the inlet
$T_{b,i}$	Fluid bulk temperature at the inlet

$T_{b,o}$	Fluid bulk temperature at the outlet
P	Perimeter of the copper tube
$\dot{m}$	Mass flow rate of the fluid in the test section
c_p	Specific heat of the fluid in the test section
A	Inner surface area of the copper tube
i	Current through the coil
R	Total resistance of the coil
F	Fraction of D.C. power used to heat fluid in the test section
D_i	Inside diameter of copper tube of heat transfer section
Nu	Nusselt number
ED	Energy density through ultrasonication.
Pr	Prandtl number
Re	Reynolds number

Greek symbols

μ_e	Effective viscosity of the dispersion
ν_p	Particle volume fraction in the dispersion
μ_m	Viscosity of the base fluid
τ	Shear stress
$\dot{\gamma}$	Shear rate
τ'	Yield shear stress

ω	Angular speed of the spindle
μ	Viscosity of the test fluid
α	Thermal diffusivity of the medium

Subscripts

c	Container
sp	Spindle
p	Particle
m	Base Fluid
s	Surface
b	Bulk
i	Inlet
o	Outlet
f	Fluid
NF	Nanofluid
w	Water

Superscripts

“	Flux
‘	At zero shear rate

Acronyms

CNT	Carbon nanotube
MWCNT	Multi-walled carbon nanotube
SWCNT	Single-walled carbon nanotube
FET	Field effect transistor
DI	De-ionized
SDS	Sodium dodecyl sulfate
SDBS	Sodium dodecyl benzene sulfonate
CTAB	Hexadecyltrimethyl ammonium bromide
GA	Gum Arabic
CTAC	Cetyltrimethylammoniumchloride
TEM	Transmission electron microscopy

TABLE OF CONTENTS

LIST OF FIGURES

FIGURE Page

FIGURE Page

CHAPTER I

INTRODUCTION

Due to rapid development in all the sectors, be it infrastructure, industrial, transportation, defense, space; managing high thermal loads has become very critical. For that reason, several cooling technologies have been researched. However, the conventional technique of heat transfer by means of a flow system including fluids like water, ethylene glycol, mineral oils had always been popular and would always remain popular due to its simple nature. Conventional heat transfer systems used in applications like petrochemical, refining, and power generation are rather large and involve significant amount of heat transfer fluids. However, in certain applications like electronics cooling in laptops and microprocessors, engine cooling in automobiles, cooling in power electronics used in military devices, cooling in space applications and many other areas, small heat transfer systems are required. These applications have a critical relationship between size of a mechanical system and the cost associated with manufacturing and operation. If improvements could be made in the existing heat transfer systems such as enhancing the performance of the heat transfer fluid, a lesser heat exchanger surface area and hence, a lesser space would be required to handle a specified amount of cooling load. The situation would lead to smaller heat transfer systems with lower capital costs and higher energy efficiencies.

This thesis follows the style of ASME Journal of Heat Transfer.

In this pursuit, numerous researchers have been investigating better techniques to enhance the thermal performance of heat transfer fluids. One of the methods used is to add nano-sized particles of highly thermally conductive materials like carbon, metal, metal oxides into the heat transfer fluid to improve the overall thermal conductivity of the fluid. The dispersion or suspension thus obtained is called as a nanofluid. These nano –sized particles could be either spherical or cylindrical. The metal and metal oxide nanoparticles are generally synthesized in spherical form, however, carbon nanoparticles could be synthesized both in spherical and cylindrical form. Of the two forms of carbon nanoparticles, the cylindrical form is more common and is called as carbon nanotubes (CNT). A type of these nanotubes is called multi-walled carbon nanotubes (MWCNT) which are more popular in heat transfer based applications.

The main focus of this work is concerned with the preparation of nanofluids by dispersing MWCNT in water and their use in heat transfer fluids. It has now been established that when carbon nanotubes are suspended in conventional heat transfer fluids, enhancements in thermal conductivity and convective heat transfer performance are observed [1-5]. The enhancement can be significant even when CNTs are added in small concentrations. The motivations behind current work are as follows. Firstly, there is limited work in studying the effect of preparation and processing conditions on the physical properties and thermal performance of CNT aqueous suspensions. This study could help in predicting optimum processing conditions to prepare effective CNT-based heat transfer fluids. Secondly, limited experimental data is currently available for CNT

based nanofluids particularly in the area of viscosity. Due to this reason, not many mathematical models are currently available to describe the flow and thermal properties of CNT nanofluids. Lastly, only two works have been reported to date on convective heat transfer of aqueous CNT nanofluids [4,6]. Convective heat transfer is an area which still needs to be completely explored and understood. All these factors will be discussed in more detail in the next chapters. In this work, an effort has been made to consider all the above factors in a study that would move forward nanofluid research to the next phase.

The thesis comprises of five chapters. The current chapter gives the introduction and the importance of the research. The second chapter is the literature review done in relevance to the past work done in nanofluid research and how it is connected to this work. The third chapter states the objectives and methodology adopted in carrying out the experiments and explains all the experimental set-ups used in the work. The fourth chapter presents and discusses the results obtained from the wet-TEM imaging, viscosity (μ), thermal conductivity (k) and convective heat transfer coefficient (h) measurements. Finally, conclusions are presented based on current work and a direction is given for future work.

CHAPTER II

LITERATURE REVIEW

In this chapter, a short background of carbon nanotubes and their physical properties relevant for heat transfer performance are presented. Additionally, a review of past work in preparing carbon nanotubes suspensions in water and measuring thermophysical properties including viscosity, thermal conductivity, and convective heat transfer coefficient of these suspensions is discussed.

2.1. Carbon nanotubes (CNTs)

Carbon nanotubes are allotropes of carbon, structured as long, thin hollow cylinders of carbon. A typical nanotube has the diameter of the order of a nanometer and the length of the order of a few micrometers. They can be thought of as a sheet of graphite (a hexagonal lattice of carbon) rolled into a cylinder. They were discovered in 1991 by S. Iijima [7]. He reported the first observation of multi-walled carbon nanotubes (MWCNT) in carbon-soot made by arc-discharge. About two years later, he made the observation of single-walled nanotubes (SWCNT) [8]. The basic structural difference between MWCNT and SWCNT is that the former has concentrically nested multiple layers of graphene structures whereas the later has only a single layer of graphene structure. These intriguing structures have given a very broad range of electronic, thermal, and mechanical properties which have sparked excitement amongst the

researchers in recent years. SWCNTs exhibit certain important electric properties which are not shared by the MWCNTs and thus are more likely candidates for miniaturizing electronics. One useful application of SWCNTs is in the development of the first intramolecular field effect transistors (FETs) [9]. On the other hand, MWCNTs have certain distinguished mechanical and thermal transport properties which make them suitable for applications related to structural composites, energy storage and heat transfer. Basic research over the past decade has shown that CNTs could have a thermal conductivity an order of magnitude higher than copper, ~3000 W/m-K for MWCNTs [10] and ~6000W/m-K for SWCNTs [11]. This suggests that CNTs have the potential to improve thermal conductivity of base fluids like water, ethylene glycol, mineral oils, etc., even when added in small quantities. Though based on the figures, SWCNTs have more potential to improve thermal conductivity; however, due to cost advantage and comparatively easy deagglomeration of MWCNTs, they have been studied more in heat transfer applications. The peculiar property of MWCNTs has made researchers interested all together in an area directed towards heat transfer-based nanotechnology applications.

2.2. Preparation of CNT nanofluids

Nanofluids are engineered colloidal suspensions of nanometer-sized (1-100nm) solid particles in conventional heat transfer fluids like water, ethylene glycol, light oils, etc. Nanofluids consisting of such particles have shown to have enhanced thermal

conductivity and convective heat transfer as compared to the base fluid [1-5]. These nanoparticles could be either metal oxides of copper, copper oxide, aluminium, alumina, titania, or they could be non-metals like carbon. In this work, we would be concentrating on carbon nanotubes dispersed in de-ionized (DI) water based on their optimal thermal properties as reported by others.

One of the critical steps in preparing carbon nanofluids is dispersing carbon nanotubes in the base fluid. Due to the high aspect ratio of carbon nanotubes and strong Van der Waal's forces between carbon surfaces, dispersion in aqueous medium can be challenging. CNTs are hydrophobic in nature and thus cannot be dispersed in water under normal conditions. Even when they are being dispersed, they have a tendency to entangle and form clusters or agglomerates. There are usually two methods to disperse carbon nanotubes in base fluids : mechanical and chemical [12]. Mechanical method such as ultrasonication can separate the nanotubes but if it is not done in a controlled way, it may physically damage the nanotubes by decreasing the corresponding aspect ratio. Chemical methods include using surfactants and CNT-functionalization using acids. The method changes the wetting or adhesion behavior which helps in reducing their tendency to agglomerate. Chemical functionalization generally involves treating the CNTs with neat acids at high temperature. This results in addition of polar groups like – COOH or – OH at defect sites on nanotube surface, thus making CNTs hydrophilic in nature. However, aggressive chemical functionalization, can damage the nanotubes. Both mechanical and chemical methods can alter the aspect ratio distribution of the

nanotubes. It has been reported that thermal conductivity enhancement in CNT nanofluids increases with aspect ratio [1,13], however, proper care still has to be taken during processing to minimize adverse effects.

In this work, a combination of mechanical method through ultrasonication, and chemical method with surfactants is used. Ultrasonication disperses particles by a series of bubble nucleation and collapse events. Ultrasonication can be done either by using an ultrasonic bath or by ultrasonic probe. Ultrasonication of fluids leads to three physical mechanisms: cavitation of the fluid, localized heating, and the formation of free radicals [12]. In the case of CNTs, this phenomenon reduces the nanotube length and reduces their tendency to entangle, which helps them disperse in a base fluid. However, even the mechanical method is not good enough to form stable suspensions. Through our experimental work, it has been found that nanotubes dispersed by just ultrasonication re-agglomerate and settle down after few days. This phenomenon results in sedimentation. This is why a chemical method involving surfactants is used as it provides milder conditions than functionalization using acids.

The surfactant gets adsorbed on the carbon nanotube surface which induces electrostatic repulsions to counterbalance Van der Waals attractions [14] between CNTs. This prevents the agglomeration of nanotubes under Van der Waal's attractions and thus provides stable suspensions. Surfactants have been used to disperse carbon nanotubes in several cases. Some examples of previously used surfactants are sodium dodecyl sulfate

(SDS) [1], sodium dodecyl benzene sulfonate (SDBS) [2], Hexadecyltrimethyl ammonium bromide (CTAB) [3] and Nanosperse AQ [3]. Through past work, it was found that SDBS failed at elevated temperatures [2]. Additionally, Gum Arabic (GA) was found to be a better surfactant than sodium dodecyl sulfate (SDS) and cetyltrimethylammoniumchloride (CTAC) for dispersing carbon nanotubes in DI water [15]. This has also been found to be confirmed from experimental work in the lab where two samples of 1 wt % MWCNT aqueous suspensions were prepared using GA and SDS as surfactants. The suspension prepared using GA was found to be visually more stable even after several weeks as compared to the one prepared using SDS. See Fig 1.

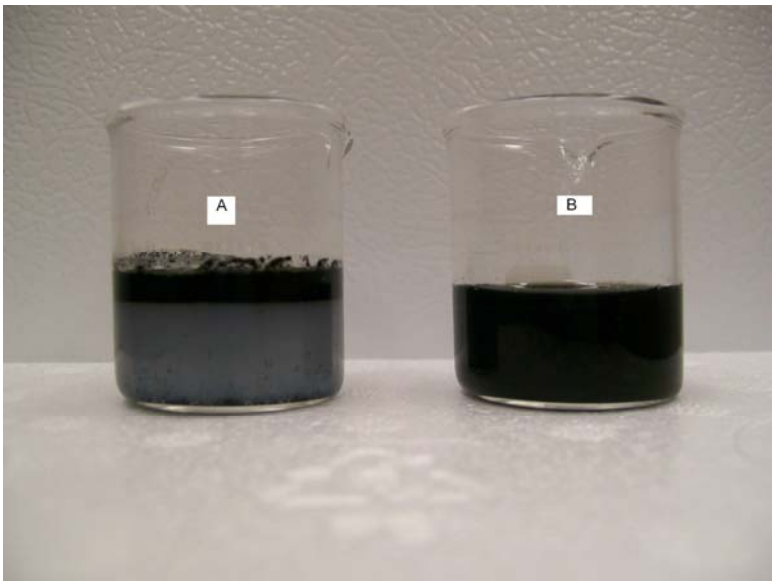

Fig. 1 Samples of 1 wt % MWCNT nanofluids after 10 weeks under room conditions of 24 °C using: (A) 0.25 wt % SDS; (B) 0.25 wt % Gum Arabic. (Note that a uniform dispersion is seen in B)

Therefore, based on past and current research, GA was found to be the most suitable surfactant. However, GA has a tendency to increase viscosity when added in small quantities to a base fluid like DI water. The high viscosity in nanofluids could result in sticking of nanotubes to the walls of the sample bottles and also to the surfaces of measuring instruments. Thus, a highly viscous nanofluid would also result in increase in pumping power for commercial applications. Therefore, it becomes important that the amount added is optimum. Through previous work [4] and also by repeated experiments in laboratory, it was found that 0.25 wt % of GA would be suitable. The method of preparation would be discussed in detail in next chapter.

2.3. Past research on viscosity of CNT nanofluids

Viscosity of a heat transfer fluid is important with respect to studying its convective heat transfer and the pumping power required for practical applications. In industry, an optimization is required between heat transfer capability and the viscosity as it has a direct bearing on the sizing of the flow and heat transfer equipment required.

Experimental data for the effective viscosity of aqueous nanofluids is limited to certain nanoparticles, such as Al_2O_3 [16-19], CuO [19, 20], TiO_2 [16] and MWCNT [4]. Most of this work has been directed towards metal oxide nanoparticles and there is only one work which studied MWCNT [4]. The parameters against which viscosity was studied were particle volume concentration, temperature and shear rate. Additionally,

understanding flow behavior of carbon nanotube(CNT) nanofluids by developing mathematical viscosity models is an important area for taking the research into the next phase. However, empirical and accurate analytical models for prediction of the viscosity of high aspect ratio nanofluids are not available at this time. The works are mainly focused on spherical nanoparticles of metal oxides, and have their basis from Einstein theory [21]. In case of CNT nanofluids, such models cannot correlate the experimental data well because the shape of CNTs does not satisfy previous assumptions. It is difficult to do particle size characterizations for CNTs and subsequently incorporate those characterizations in the Einstein viscosity model (Eq. 2.1).

$$\mu_e = (1 + 2.5\nu_p)\mu_m \qquad (2.1)$$

Where μ_e, ν_p and μ_m are effective viscosity of the dispersion, particle volume fraction in the dispersion, and viscosity of the base fluid, respectively.

Aqueous CNT nanofluids have shown to exhibit shear thinning or pseudoplastic type of non-Newtonian behavior [4]. However, no work has been done in correlating this behavior to theoretical non-Newtonian viscosity models. The theoretical models provide equations to correlate shear stress of a flowing fluid to shear rate. This could help in classifying the flow behavior of a new nanofluid under the already studied behavior of fluids, and thus help in directing future rheological studies. The widely used models for non-Newtonian flow are Power Law (Eq 2.2) and Herschel Bulkley (Eq. 2.3).

$$\tau = K.\dot{\gamma}^{n} \quad (2.2)$$

$$\tau = \tau' + K.\dot{\gamma}^{n} \quad (2.3)$$

Where $\tau, K, \dot{\gamma}, \tau'$ and n are shear stress, flow consistency index, shear rate, yield shear stress and flow behavior index, respectively. The value of parameters 'K' and 'n' signify the flow behavior in quantitative and qualitative terms respectively. A high value of 'K' is attributed to high viscous behavior and a low value (less than 1 for pseudoplastic fluids) of 'n' is attributed to high degree of non-Newtonian behavior of the fluid.

Additionally, no work has been done in studying the effect of processing or ultrasonication time on the viscosity of MWCNT aqueous suspensions or nanofluids. Experimental work in this area could provide impetus to theoretical model development for CNT nanofluids. In this work, an effort has been made to study this effect and subsequently fitting the experimental data in the form of a shear stress- shear rate mathematical equation.

2.4. Past research on thermal conductivity of CNT nanofluids

The heat transfer characteristic of a flowing fluid can be represented by a Nusselt number, which takes into account the fluid thermal conductivity directly and indirectly

through the Prandtl number. Thus, a first assessment of the heat transfer potential of a nanofluid is to measure its thermal conductivity. To date, a lot of research has been published in this area for metal oxide nanofluids but comparatively less for CNT nanofluids [17, 22, 23]. One of the first works involving CNT nanofluids was by Choi et al. [5]. They measured the effective thermal conductivity of MWCNTs dispersed in synthetic poly(α-olefin) oil and reported a thermal conductivity enhancement of 160% by 1.0 vol % nanotubes in oil. Subsequently, data was published by Xie et al. [24] where enhancements were reported for water, ethylene glycol and decene as base fluids. Assael et al. [1, 3] data focused on aqueous MWCNT nanofluids with SDS, CTAB and Nanosperse AQ as dispersants. However, both these works reported much less enhancements as compared to those reported by Choi et al. [5]. The maximum thermal-conductivity enhancement observed by Xie et al. [24] was only 20% for 1% nanotubes in decene by volume, and that observed by Assael et al. [1] was 38% for 0.6% CNTs in water by volume. In 2004, Wen and Ding [2] published data using SDBS as the dispersant. Their results were comparable to Xie et al. [24] and Assael et al. [1] and proposed differences in the interfacial resistances and thermal conductivities of carbon nanotubes used in these studies as the main reasons for the observed discrepancies with respect to Choi et al. [5]. Additionally, the base fluid used by Choi et al. [5] was poly-α-olefin (a lower thermal conductivity than water), though percentage enhancement reported was high, the absolute enhancement was not as high as expected. As SDBS was also found to fail at elevated temperatures, in 2006, another set of data was published

using GA as dispersant by Ding et al. [4]. In this work, a maximum enhancement of 79% was reported at 1 wt % MWCNT in water.

To date, most of the published data in MWCNT based nanofluids is focused on the thermal conductivity enhancement with parametric effects of particle volume concentration, base fluid, and temperature. Though parametric effects of particle size [1, 3], dispersant (surfactant) [1, 3] and acidity [4] have been considered, only a few papers have been published in this area. As nanotubes are cylindrical in nature and exist as agglomerates, direct particle size characterization using techniques like Dynamic Light Scattering (DLS) is difficult for nanotubes. Assael et al. [3] reported the effect of particle size indirectly by increasing the ultrasonic homogenization time and concluded that when carbon nanotube suspensions are homogenized for long periods of time, their aspect ratio decreases, which subsequently decreases their thermal conductivity enhancements. However, no other work has been found to confirm these findings. In the present work, an effort was made by measuring the thermal conductivity enhancements with respect to ultrasonication time and temperature.

The reason behind thermal conductivity enhancement in carbon nanotube dispersions is still not completely understood. There are many phenomena postulated for the enhancement. Studies have indicated that nanotubes conduct current and heat ballistically or in fast diffusive manner [11]. The ballistic conduction is associated with the large phonon mean-free path in nanotubes. Hence, nanotubes change the cause of

heat conduction from diffusion in liquids to both fast diffusion and ballistic heat conduction in nanofluids. Furthermore, there is evidence that an organized solid-like structure of a liquid at the interface is a governing factor in heat conduction from a solid wall to an adjacent liquid [25]. Therefore, it has been postulated [5] that this organized solid/liquid interface structure causes the energy transport across the interface. Additionaly, in 2004, Jang and Choi [26] postulated another theory using Brownian motion of nanoparticles as a potential factor for increased thermal conductivity of nanofluids at elevated temperatures. It suggested that as temperature is increased, the viscosity of base fluids is decreased and the Brownian motion of nanoparticles is consequently increased. It has been postulated that convection like effects are induced by Brownian motion which result in increased conductivities. However, previously Keblinski et al. [27] showed that Brownian motion is unlikely to have direct role in the enhancement of thermal conductivity. Wen and Ding [2] suggested nanotube networking as one of the likely mechanisms that facilitates avenues for ballistic transport of energy carriers. From all these works, it is difficult to agree upon a single most important mechanism that solely contributes to enhanced thermal conductivity.

2.5. Past research on convective heat transfer of CNT nanofluids

The benefit of nanofluids as heat transfer fluids is best determined by its convective heat transfer coefficient. Unlike research in the area of thermal conductivity, the study of convective heat transfer of nanofluids still needs to be explored in more detail. Only a

few papers have been written in this area and most of them focused on metal oxide nanoparticles [15,18,21,22]. To date, only two works have been published that considered using MWCNT aqueous suspensions, and both of them studied heat transfer under laminar flow conditions. Faulkner et al. [6] reported heat transfer enhancement in a microchannel at very low Reynolds number (2-17) and particle volume concentrations between 1.1-4.4 vol %. Ding et al. [4] reported heat transfer enhancement at intermediate Reynolds number (800-1200) and low particle volume concentration (0.05 vol %). Although both of these papers reported heat transfer enhancement, however, the heat transfer enhancement trends with respect to particle volume concentration in one paper was found to contradict the other work. Therefore, it can be said that substantial amount of work is still required in this area. Both these papers considered parametric effects of particle volume concentration, Reynolds number and heat flux on the heat transfer enhancement. However, ultrasonication time or particle size reduction was not considered in those studies.

As experimental research in this area is still new, theoretical models for heat transfer enhancement are quite limited too. Most of the work is reported is in the turbulent flow regime and none of them has been modeled using MWCNT aqueous suspensions as the test fluid.

CHAPTER III

EXPERIMENTAL DESIGN

This section explains the objectives, the description of the experimental set-ups used to measure viscosity, thermal conductivity and convective heat transfer coefficient of the samples, and the steps involved in the preparation of aqueous suspensions of MWCNT.

3.1. Objectives and methodology

The overall purpose of this research was to study the effect of ultrasonication on viscosity and heat transfer performance of aqueous suspensions of multi-walled carbon nanotubes. To satisfy the overall objective of this research, the following tasks are were undertaken:

1. Prepared four samples of aqueous suspensions of 1 wt% multi-walled carbon nanotubes using ultrasonication method for different amount of processing time including 20 minutes, 40 minutes, 60 minutes and 80 minutes.

2. In-situ microscopic pictures of the four samples were taken using wet-TEM imaging technique.

3. Measured the viscosity of each of these samples using a rotating spindle Brookfield viscometer under low temperature condition (i.e. 15 °C) and high temperature condition (i.e. 30 °C) at several shear rates.

4. Compared these viscosity values with those of the base fluid comprising of 0.25 wt% Gum Arabic and DI water, to find out the relative change in viscosity under different ultrasonication time and the impact of MWCNT addition.

5. Compared the experimental data with the theoretical viscosity models to classify the flow behavior of CNT nanofluids.

6. Measured the thermal conductivity of each of the samples using KD 2 Pro Thermal Properties Analyzer, under varying conditions of temperature including 15 °C, 24 °C, 30 °C and 35 °C.

7. Compared these thermal conductivity values with that of DI water to find out the relative enhancement in thermal conductivity under different ultrasonication time and the impact of MWCNT addition.

8. Measured the convective heat transfer coefficient of each of the samples under laminar flow and constant heat flux conditions, by using a well-calibrated heat transfer section.

9. Compared these convective heat transfer coefficient values with that of DI water to find out the relative enhancement in thermal conductivity under different ultrasonication time and the impact of MWCNT addition.

3.2. Set-up description

This section describes the working principle involved behind each of the experimental set-ups used for preparing sample and measuring viscosity, thermal conductivity, and convective heat transfer coefficient.

3.2.1. Ultrasonication probe

The ultrasonic processor used for sample preparation was 130 watts, 20 kHz ultrasonication probe from Sonics & Materials, Inc. According to the operator's manual of the instrument, the processor's power supply converts 60 Hz line voltage to a high frequency electrical energy. The high frequency electrical energy is changed into mechanical vibrations through a piezoelectric transducer. The vibrations when being transmitted through the probe are further intensified and create pressure waves in the liquid sample. The induction of pressure waves forms several microscopic bubbles inside the sample, which expand during negative pressure excursion and implode violently during the positive excursion. As the bubbles implode, they cause several shock waves and eddies that radiate outwardly from the site of collapse, and also

generate extremes in pressures and temperatures at the implosion sites. Although this phenomenon, known as cavitation, lasts few microseconds, and the amount of energy released by each individual bubble is minimal, however, the cumulative amount of energy generated is extremely high. See Fig. 2 for the set-up picture.

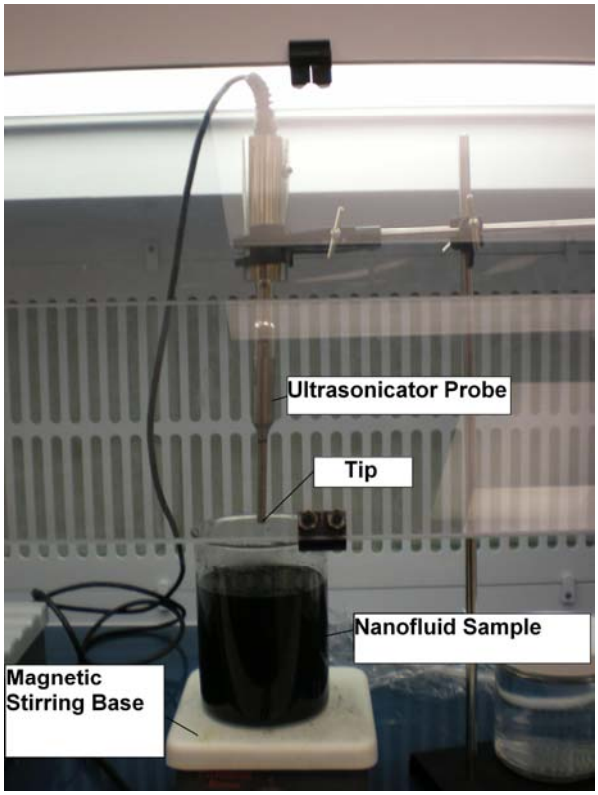

Fig. 2 Ultrasonication probe set-up.

3.2.2. Wet-TEM

Carbon nanotubes(CNTs) due to their nanometric scale are difficult to image by conventional microscopic imaging techniques. Therefore, to capture pictures of carbon

nanotubes, transmission electron microscopy (TEM) is used. However, one of the limitations of the usual TEM technique is that the test sample has to be dried and exposed to vacuum before it can be imaged. Using the conventional TEM technique, CNT dispersions are dried to prepare samples, which induces structural changes in the sample as compared to the original test fluid. Therefore, one can never be sure whether the dried test sample is representative of the original sample. To overcome this problem, a new type of TEM technique is available known as wet-TEM. Wet-TEM as the name suggests allows imaging the sample under wet or *in-situ* conditions without altering the original test fluid. This facilitates to image the actual quality of dispersion of carbon nanotubes within the base fluid.

A wet-cell TEM technique developed by Dongxiang Liao and Jianguo Wen from the Frederick Seitz Materials Research Laboratory at the University of Illinois at Urbana-Champaign was used [28]. The CNT samples prepared in the laboratory were sent to Construction Engineering Research Lab (CERL), Engineer Research and Development Center (ERDC), Champaign, IL for imaging. A JEOL 2010 LaB6 TEM was used with a beam acceleration voltage of 200 keV. The wet-cell was constructed by holding the fluid between two silicon nitride membrane window TEM grids. The grids contained a 200 μm thick frame and a 50 nm thick window, in which the sample was placed. Thus, even a tiny drop of the sample could be used. The grids were then placed in a custom-built TEM sample holder that included a number of o-rings intended to create a seal against the vacuum for the fluid in the grid. See Fig. 3.

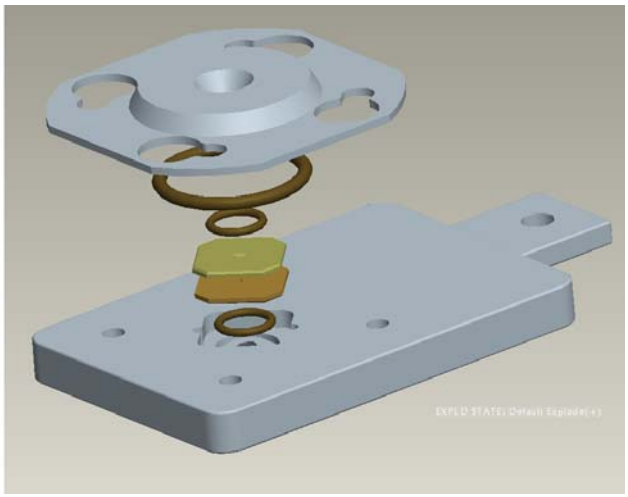

Fig. 3 Exploded view of wet-cell assembly.
(Source: Franks et al., 2008 [28])

3.2.3. Viscometer

The viscometer used was from Brookfield Engineering Laboratories, Inc. It was of the rotational variety. According to the operator's manual of the instrument, the instrument measures the torque required to rotate an immersed element (the spindle) in a fluid. The spindle is driven by a motor through a calibrated spring; deflection of the spring is converted internally through a set of formulae to display the dynamic viscosity in centipoises (cP). By utilizing a multiple speeds and different spindles, a variety of viscosity ranges can be measured. For a given viscosity, the viscous drag (indicated by the degree to which the spring winds up), is proportional to the spindle's speed of rotation and is related to the spindle's size and shape. The drag will increase as the spindle size and/or rotational speed increase. It follows that for a given spindle geometry

and speed, an increase in viscosity will be indicated by an increase in deflection of the spring. Measurements made using the same spindle at different speeds are used to detect and evaluate rheological properties of the test samples. The model used in the laboratory was meant for low viscosity fluids and had a maximum torque rating of 0.06737 milli Newton-m. The instrument had an specified accuracy of ± 1%, which was verified using a Brookfield's standard viscosity test fluid. A combination of cylindrical sample container and spindle called as UL Adapter was used for the measurements. The UL Adapter is an attachment provided with the instrument for taking measurements on low viscosity test samples. The viscous drag experienced by the spindle in UL Adapter is calibrated to display dynamic viscosity and percentage of maximum torque by using Eq.3.1-3.4. See Fig. 4 and Fig. 5 for the dimension parameters and set-up picture, respectively.

$$\dot{\gamma} = \frac{(2.R_c^2)}{(R_c^2 - R_{sp}^2)}.\omega \qquad (3.1)$$

$$\tau = \frac{M}{2\pi R_{sp}^2 L} \qquad (3.2)$$

$$\mu = \frac{\tau}{\dot{\gamma}} \qquad (3.3)$$

$$\omega = \frac{2\pi N}{60} \tag{3.4}$$

Where $R_c, R_{sp}, \omega, M, L, \mu$ and N are radius of the sample container, radius of the spindle, angular speed of the spindle, torque input by the viscometer, effective length of the spindle, dynamic viscosity and rotational speed of the spindle, respectively.

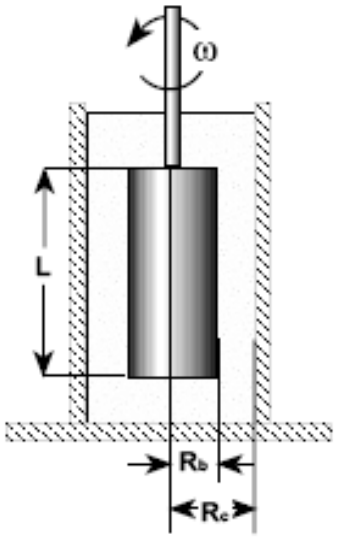

Fig. 4 Diagram to explain the dimension parameters.
(Source : More Solutions to Sticky Problems, Brookfield Inc., USA)

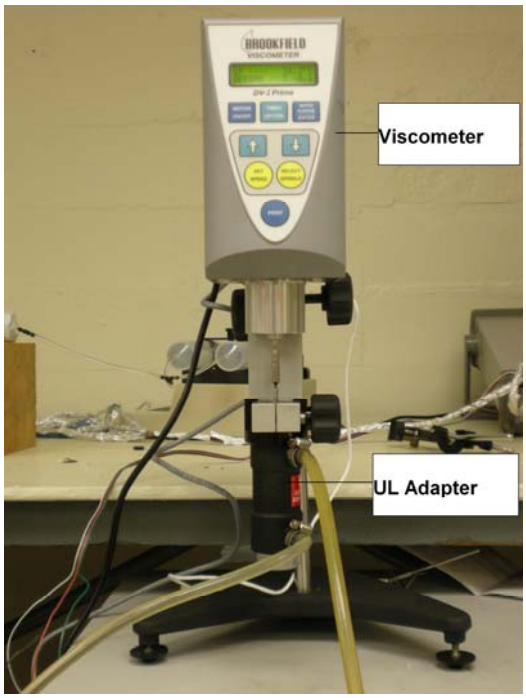

Fig. 5 Set-up for viscosity measurements using Brookfield viscometer.

3.2.4. Thermal conductivity analyzer

The thermal conductivity was measured by using a KD 2 Pro thermal properties analyzer from Decagon devices, Inc. The instrument had a probe of 60 mm length and a 1.3 mm diameter and included a heating element, a thermo-resistor and a microprocessor to control and measure the conduction in the probe. The instrument had a specified accuracy of 5%. The measurements were taken under different temperature conditions by using a temperature-controlled chiller. A number of measurements were taken for each sample and a mean of only those measurements with '$R^{2'}$ value, square of

correlation coefficient, greater than 0.9995 were considered. The instrument was based on the working principle of a transient hot wire method used in past works [1, 3, 4, 29].

The method requires a constant amount of heat be applied to a zero mass heater over a period of time in an infinite medium, rather than as an instantaneous pulse. According to theory given in the operator's manual of the instrument, the temperature response, ΔT for $0 < t \le t_1$ is defined as:

$$\Delta T = -\frac{\dot{q}}{4\pi k} Ei\left(\frac{-r^2}{4\alpha t}\right) \tag{3.5}$$

The temperature rise, ΔT after the heating has been turned off, for $t > t_1$ is defined as:

$$\Delta T = -\frac{\dot{q}}{4\pi k}\left[-Ei\left(\frac{-r^2}{4\alpha t}\right) + Ei\left(\frac{-r^2}{4\alpha\left(t-t_1\right)}\right)\right] \tag{3.6}$$

where $\dot{q}, k, Ei, r, t, \alpha$ and t_1 are rate of heat dissipation, thermal conductivity of the medium, exponential integral, radial distance from the heating source, time, thermal diffusivity and heating time, respectively.

Material thermal properties including thermal conductivity and thermal diffusivity are determined by fitting the time series temperature data during heating to Eq. 3.5, and

during cooling to Eq. 3.6 by using a non-linear least square procedure explained in the literature provided with the instrument. The algorithm for the method has been integrated within the instrument itself, and the user gets the thermal conductivity and correlation coefficient directly displayed on the screen. See Fig. 6 for the set-up picture.

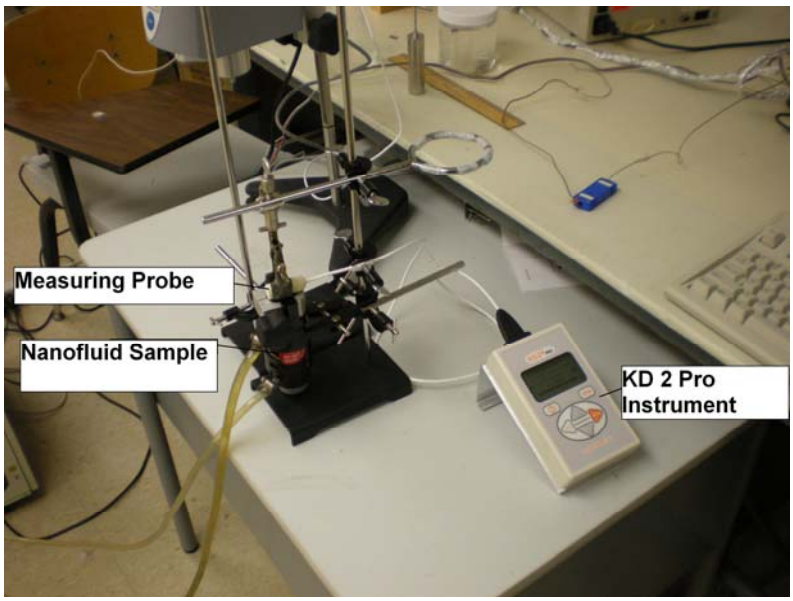

Fig. 6 Set-up for thermal conductivity measurements using KD 2 Pro Thermal Properties Analyzer.

3.2.5. Convective heat transfer section

The experimental set up used to measure convective heat transfer coefficient was similar to the one used by Ding et al [4], and is shown schematically in Fig. 7. The set-up was calibrated to give measurements within 5 % accuracy. It consisted of a copper heat transfer section, Agilent data acquisition system, a D.C. power supply, a syringe

metering pump and a computer. A straight copper tube of 914.4 mm length, 1.55 mm inner diameter and 3.175 mm outer diameter was used as a test section.

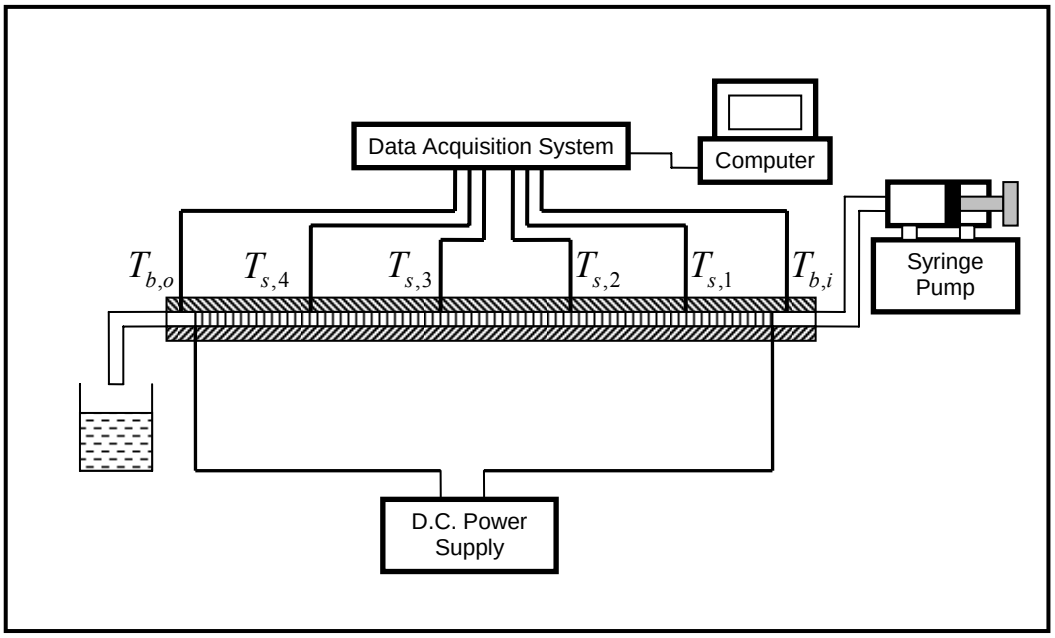

Fig. 7 Schematic for convective heat transfer measurement experimental set-up.

The whole section was heated by an AWG 30 nichrome 80 wire (MWS wire industries, USA) wound on the tube and connected to a 1500 W, 0-300V, 0-5A D.C. power supply (Lambda, U.S.A.). The experiments were run under constant heat flux conditions using a current of 0.2 A. The test section was insulated to prevent loss of heat to the surroundings. Four surface-mount thermocouples were mounted on the test section at axial positions of 19 mm ($T_{s,1}$), 39.5 mm ($T_{s,2}$),59 mm ($T_{s,3}$) and 79 mm ($T_{s,4}$) from the inlet of the section to measure surface or wall temperature distribution. Additionally, two thermocouples were mounted at the inlet and outlet to measure the bulk temperature of

the flowing medium at inlet and outlet, respectively. The pump used was a Cole Palmer syringe metering pump. The flow rates used were 40 mL/min, 60 mL/min and 80 mL/min such that the flow conditions are always laminar. The corresponding Reynolds number for water at these flow rates are approximately 600, 900 and 1200, respectively. All the thermocouples and the output from the D.C. power supply were connected to a Data Acquisition system (Agilent 34970A), which is further connected to a computer (AMS, Pentium IV). See Fig. 8 for the set-up picture.

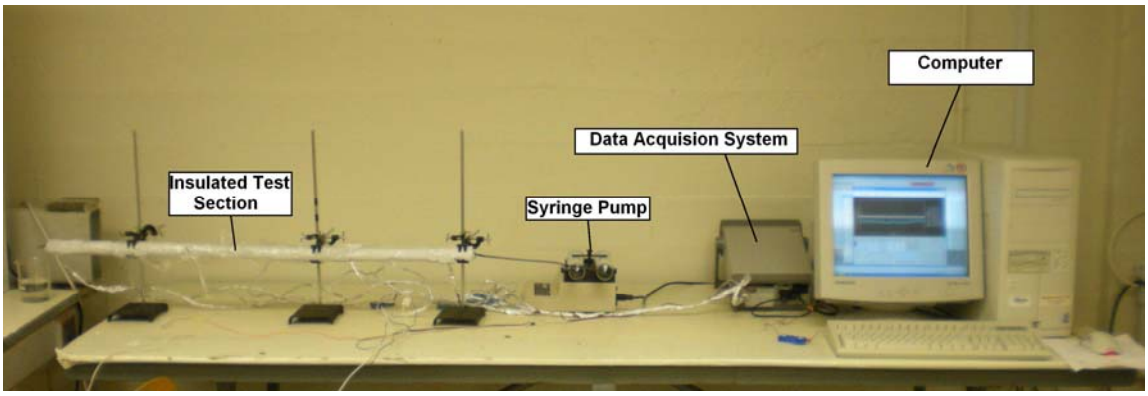

Fig. 8 Set-up for convective heat transfer measurement.

The set-up was calibrated both under isothermal and constant heat flux operating conditions. The calibration method used is explained in Appendix B.

The convective heat transfer coefficient at an axial distance 'x' from inlet is defined as:

$$h(x) = \frac{q_s''}{T_s(x) - T_b(x)} \qquad (3.7)$$

Where $q_s^{"}, T_s(x)$ and $T_b(x)$ are heat flux applied to the fluid, surface or wall temperature at a distance 'x' from the inlet, and fluid bulk temperature at a distance 'x' from the inlet, respectively.

From energy balance equation, assuming linear variation, the bulk temperature of the fluid at an axial distance, x is defined as:

$$T_b(x) = T_{b,i} + \frac{q_s^{"}.P}{\dot{m}.c_p}.x \qquad (3.8)$$

Where $T_{b,i}, P, x, \dot{m}$ and c_p are fluid bulk temperature at the inlet, perimeter of the copper tube, axial distance from the inlet of the test section, mass flow rate of the fluid, and specific heat of the fluid respectively.

The heat flux through the copper tube is defined as:

$$q_s^{"} = \frac{\dot{m}.c_p(T_{b,o} - T_{b,i})}{A} \qquad (3.9)$$

Which is same as

$$q_s^{"} = \frac{F.\left(i^2.R\right)}{A} \tag{3.10}$$

where $T_{b,o}, A, F, i$ and R are fluid bulk temperature at the outlet, inner surface area of the copper tube, fraction of DC power used to heat fluid, current through the coil, and the total resistance of the coil, respectively. 'F' was found from Eq. 3.9 and Eq. 3.10 and was found to be nearly '0.8' for the set-up. It gave an idea of heat losses.

The convective heat transfer coefficient is also defined in the form of Nusselt number (Nu) as:

$$Nu(x) = \frac{h(x).D_i}{k} \tag{3.11}$$

Where, D_i is the inside diameter of the copper tube.

3.3. Sample preparation

De-ionized (DI) water, Gum Arabic (GA) and multi-walled carbon nanotubes (MWCNT) were used to produce the aqueous suspensions. The nanotubes were procured from Helix Material Solutions Inc, USA. The nanotubes had a specified average outside diameter of 10-20 nm, length of 0.5-40 μm and purity of 95 %. The nanotubes were

produced by chemical vapor deposition (CVD) process. Gum Arabic was from Biochemika in fine powder form.

The sample preparation set-up was kept in a fume hood to prevent contamination of nanofluids and as a safety precaution. See Fig. 9 for the set-up picture. Each sample was prepared by dissolving 1.25 gm of GA in 493.75 gm of DI water using magnetic stirring until a homogenous looking solution was obtained. After that, 5 gm of MWCNT was added to the solution. The composition gave a 500 gm sample with mass percentage of GA and MWCNT as 0.25 % and 1% respectively. The resulting composition was ultrasonicated for 5 minutes at 100 % amplitude using an ultrasonication probe until a black homogenous looking suspension was obtained. This was followed by 5 minutes of magnetic stirring.

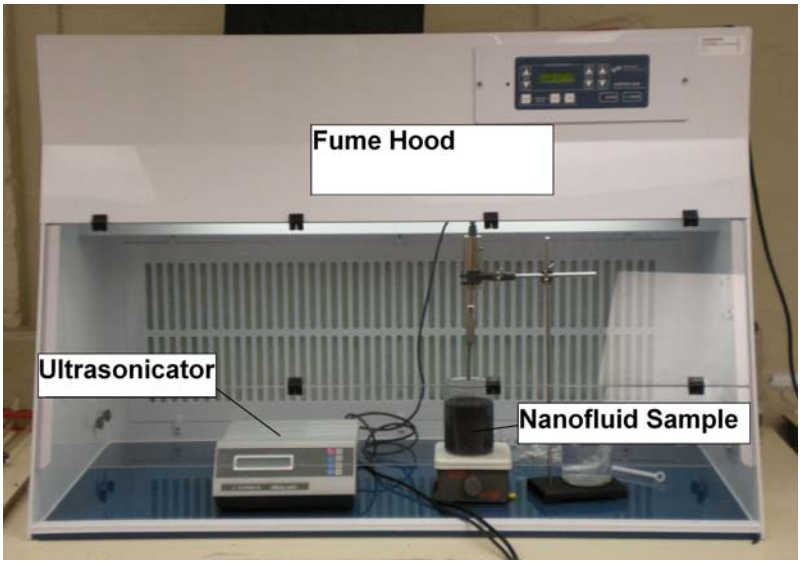

Fig. 9 Set-up for nanofluid preparation.

The ultrasonication and magnetic stirring process were alternated every 5 minutes until the sample had been sonicated for desired amount of time. Four samples were prepared with mass fraction of GA and MWCNT as 0.25 % and 1 % respectively, however with varying ultrasonication times. Based on processing time, a certain amount of energy was transferred to each sample. This energy was divided by the mass of the sample (i.e. 500gm) to obtain the energy density, ED provided to each sample. It was assumed that all the energy was imparted to the fluid.

Therefore, the samples are defined as:

a) Sample A: 1 wt % MWCNT, 0.25 wt % GA, ultrasonicated for 20 minutes, ED = 57 J/g.
b) Sample B: 1 wt % MWCNT, 0.25 wt % GA, ultrasonicated for 40 minutes, ED = 113 J/g.
c) Sample C: 1 wt % MWCNT, 0.25 wt % GA, ultrasonicated for 60 minutes, ED = 188 J/g.
d) Sample D: 1 wt % MWCNT, 0.25 wt % GA, ultrasonicated for 80 minutes, ED = 290 J/g.

The samples prepared by this technique were found to be stable for over one month with no visible sedimentation or settling. See Fig. 10. From the figure, a uniform dispersion (indicative of a single phase) was observed in all the samples.

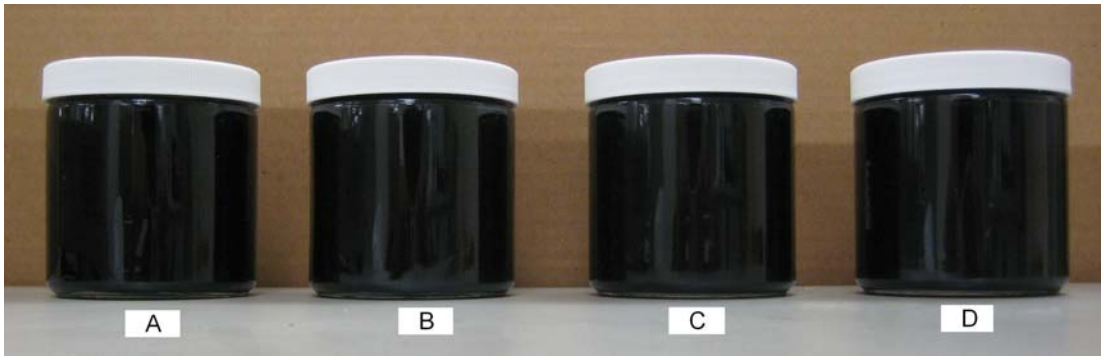

Fig. 10 Vials containing aqueous suspensions of 1 wt % MWCNT after 1 month of sonication for different times: (A) 20 minutes; (B) 40 minutes; (C) 60 minutes; (D) 80 minutes.

3.4. Summary of experiments

The summary of experimental investigations performed on the samples has been provided in the Table1.

Table 1 List of Experiments.

Imaging	Viscosity Measurements	Thermal Conductivity Measurements	Convective Heat Transfer Measurements
In-situ imaging of sample using wet-TEM	At 15 ^{o}C and 30 ^{o}C at different shear rates.	At 15 ^{o}C, 24 ^{o}C , 30 ^{o}C and 35 ^{o}C	Under laminar and constant heat flux conditions, with Re ~ 600, 900 and 1200

CHAPTER IV

RESULTS AND DISCUSSION

This chapter presents the data obtained from viscosity measurements, thermal conductivity measurements and convective heat transfer measurements, and discusses these results in context of fundamental theory and past research.

4.1. Imaging data

Figures 11-14 show the pictures of Samples A, B, C and D (prepared as described in section 3.3) at a scale of 0.5 μm, under *in-situ* conditions, using wet-TEM technique.

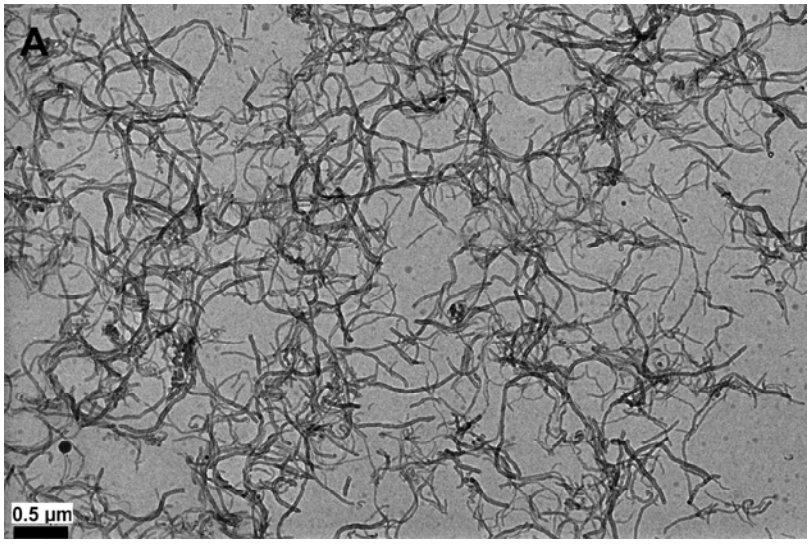

Fig. 11 Wet-TEM image of Sample A at 0.5 μm scale. (1 wt % MWCNT, 0.25 wt % GA, 20 min sonication)

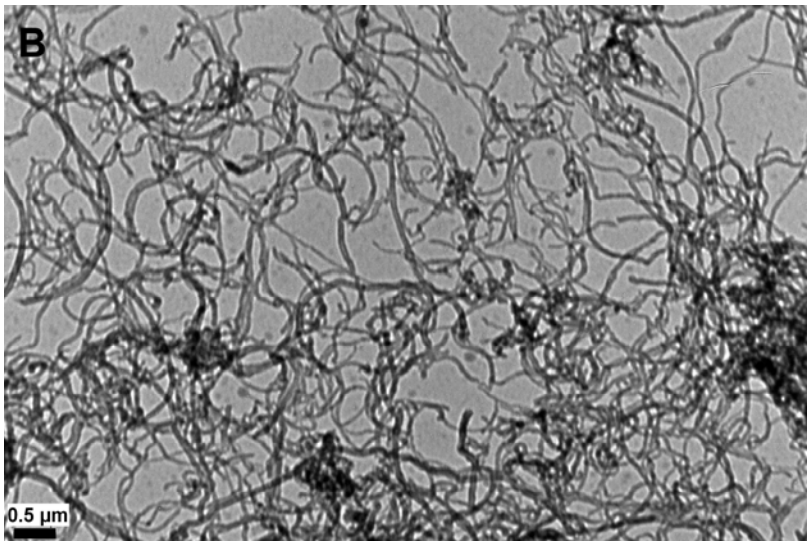

Fig. 12 Wet-TEM image of Sample B at 0.5 µm scale. (1 wt % MWCNT, 0.25 wt % GA, 40 min sonication)

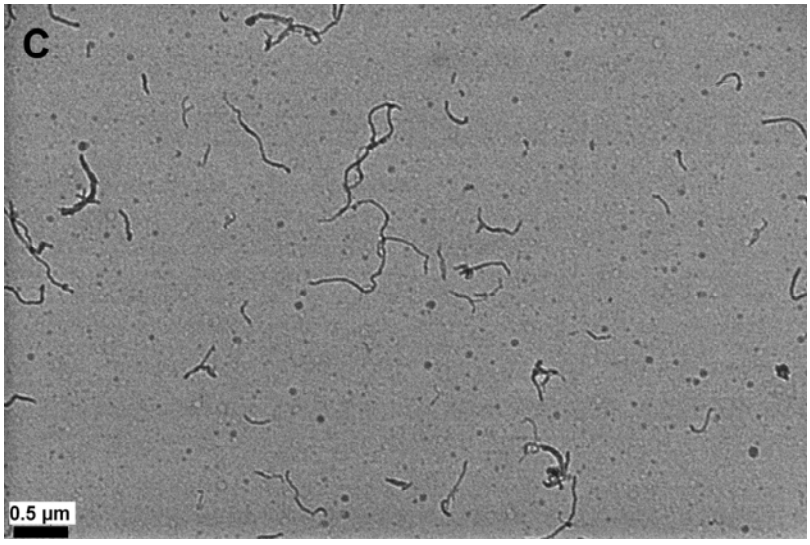

Fig. 13 Wet-TEM image of Sample C at 0.5 µm scale. (1 wt % MWCNT, 0.25 wt % GA, 60 min sonication)

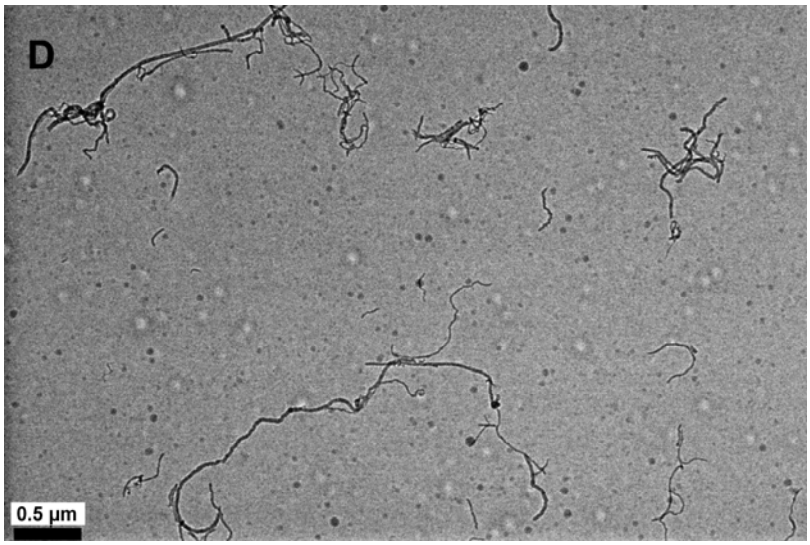

Fig. 14 Wet-TEM image of Sample D at 0.5 µm scale. (1 wt % MWCNT, 0.25 wt % GA, 80 min sonication)

From Fig. 11 and 12, it can be seen that Samples A and B exhibit a good three-dimensional network of carbon nanotubes. In contrast, from Fig. 13-14 of Samples C and D, it can be seen that the nanotubes are loosely placed without a uniform network. This observation can be attributed to more ultrasonic processing in case of Samples C and D.

This can be further explained in more detail by comparing Samples B and D. From Fig. 15 and 16 after having a closer look at a scale of 200 nm, it can be seen that the length of the nanotubes has somewhat decreased in Sample D as compared to Sample B. The greater ultrasonic processing time (i.e. 80 minutes) in Sample D as compared to lesser ultrasonic processing time (i.e. 40 minutes) seems to have altered the length. A decrease in length decreases the aspect ratio of nanotubes.

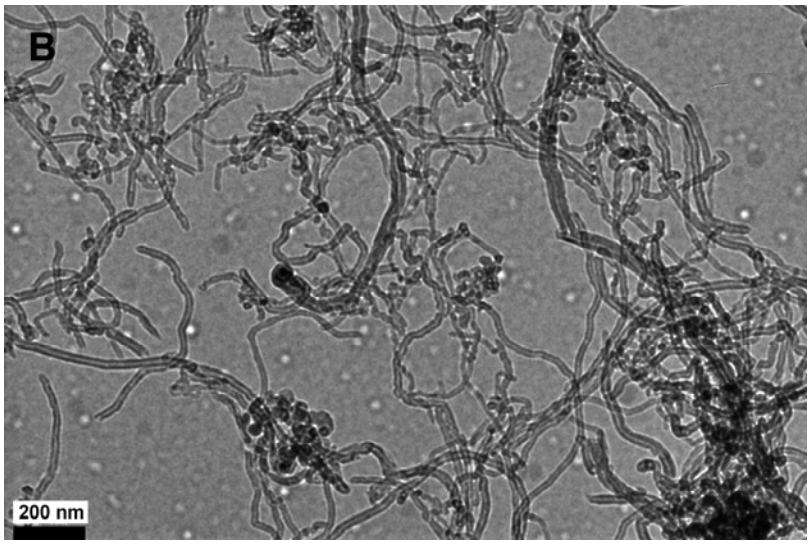

Fig. 15 Wet-TEM image of Sample B at 200 nm scale. (1 wt% MWCNT, 0.25 wt % GA, 40 min sonication)

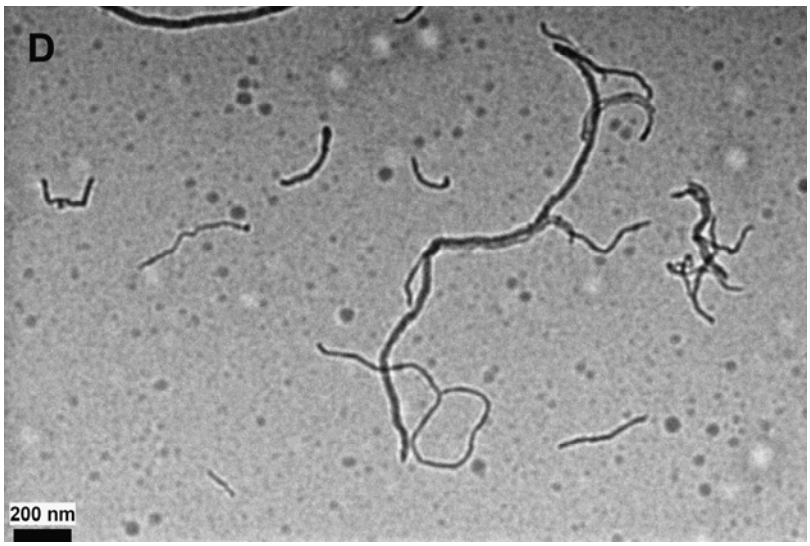

Fig. 16 Wet-TEM image of Sample D at 200 nm scale. (1 wt% MWCNT, 0.25 wt % GA, 80 min sonication)

It can be seen from Fig. 12,14, 15 and 16 that the alteration in aspect ratio has affected the quality of three-dimensional network which is found to be denser in Sample B than in Sample D.

The imaging data would be related to the flow and thermal properties of each sample in the subsequent sections of this chapter.

4.2. Viscosity data

As discussed in the last section, the viscometer used is of rotating type. Hence, the shear rate is produced by a spindle rotating at a certain rotational speed, N (rpm). This rotational speed has been converted to provide shear rate, $\dot{\gamma}$ (sec^{-1}) in Appendix A. Figure 17 shows the variation of dynamic viscosity with shear rate for each of the samples including 0.25 wt % GA and water at temperatures of 15 °C.

It can be clearly seen from both of these figures that that carbon nanotube aqueous suspensions display a non-Newtonian behavior because viscosity changes with shear rate. A shear thinning or pseudoplastic behavior was observed resulting in a decrease in viscosity with increase in shear rate. In case of 0.25 wt % GA, shear thinning was observed which gets transformed into a slight shear thickening or dilatant behavior at high shear rate. A shear thinning effect can be explained by possible de-agglomeration

of bundled nanotubes and/or realignment in the direction of the shearing force, resulting in less viscous drag.

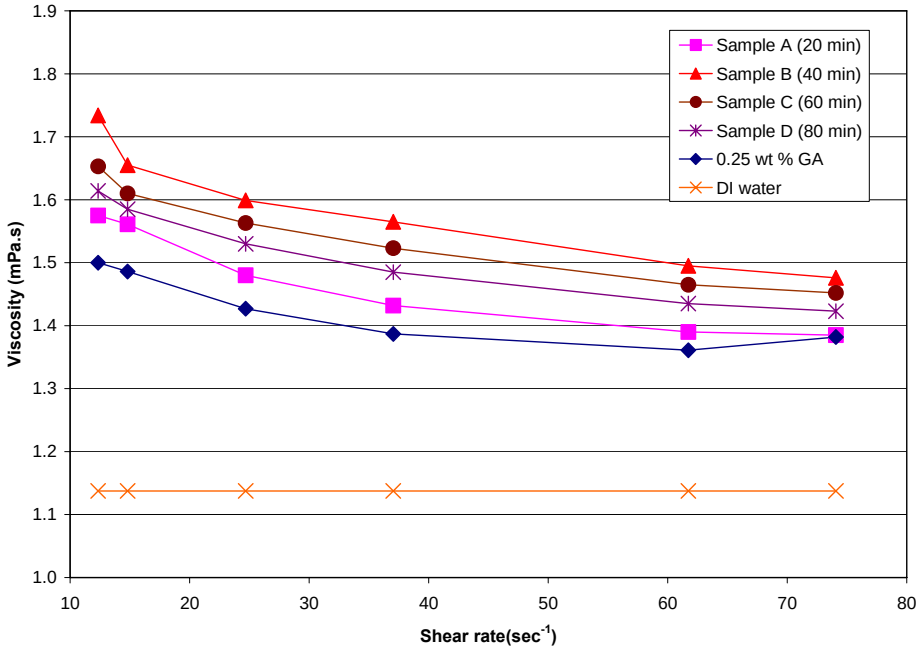

Fig. 17 Variation of dynamic viscosity with shear rate at 15 °C.

Similar plot could be seen at a temperature of 30 °C in Fig. 18.

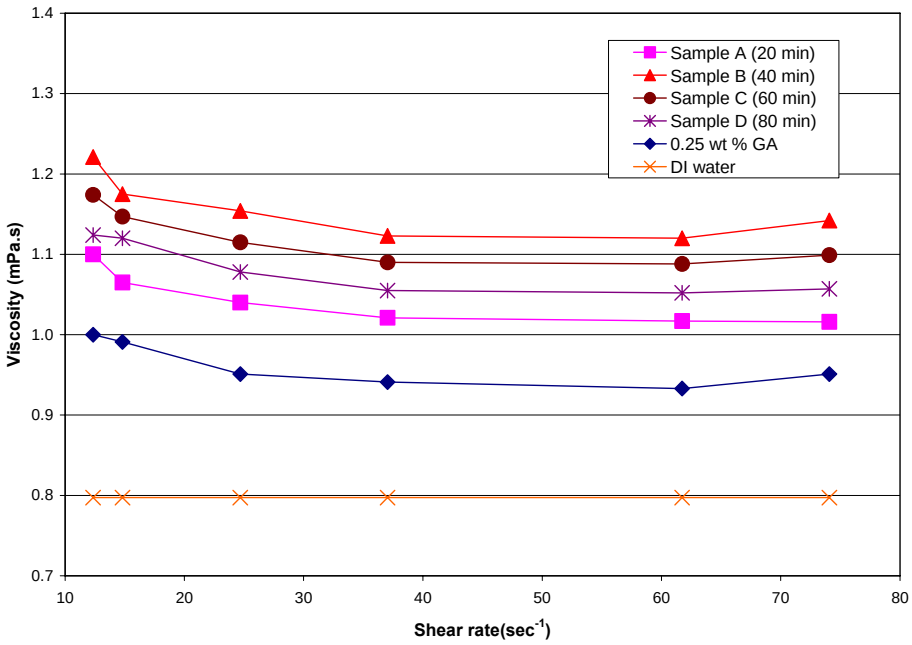

Fig. 18 Variation of dynamic viscosity with shear rate at 30 °C.

The similar phenomenon was also reported by Ding et al [4]. A normalized characterization of this behavior is shown in Fig. 19 and 20, where relative viscosity of each sample with respect to a solution of 0.25 wt % Gum Arabic is plotted at the two temperatures.

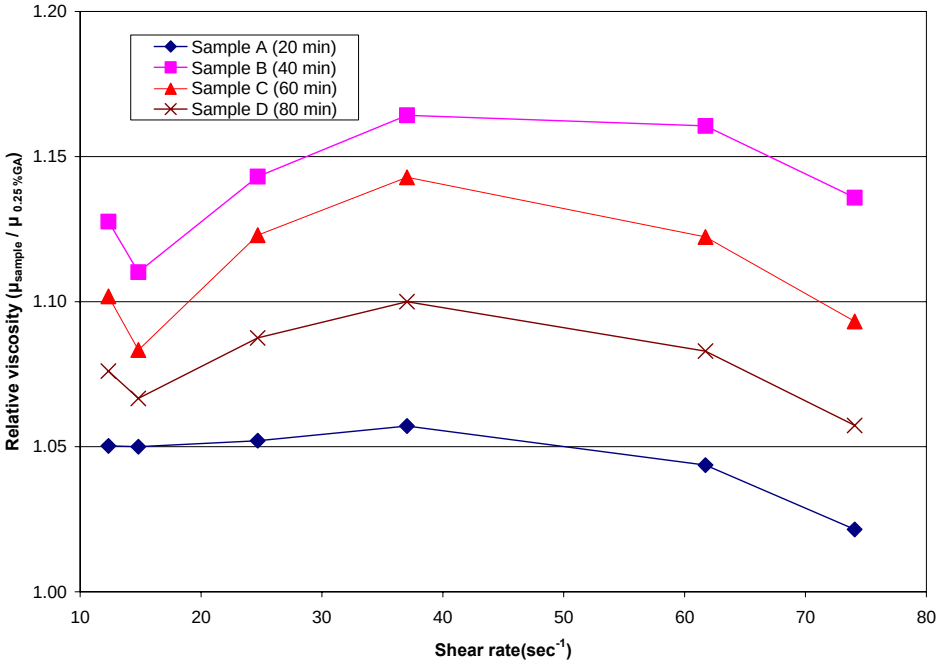

Fig. 19 Variation of relative viscosity with shear rate at 15 °C.

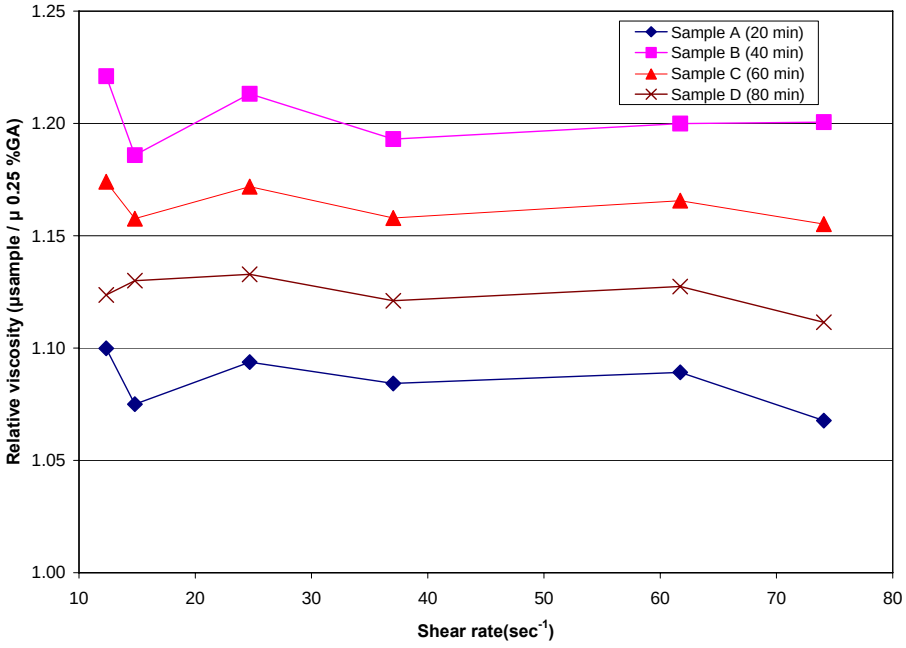

Fig. 20 Variation of relative viscosity with shear rate at 30 °C.

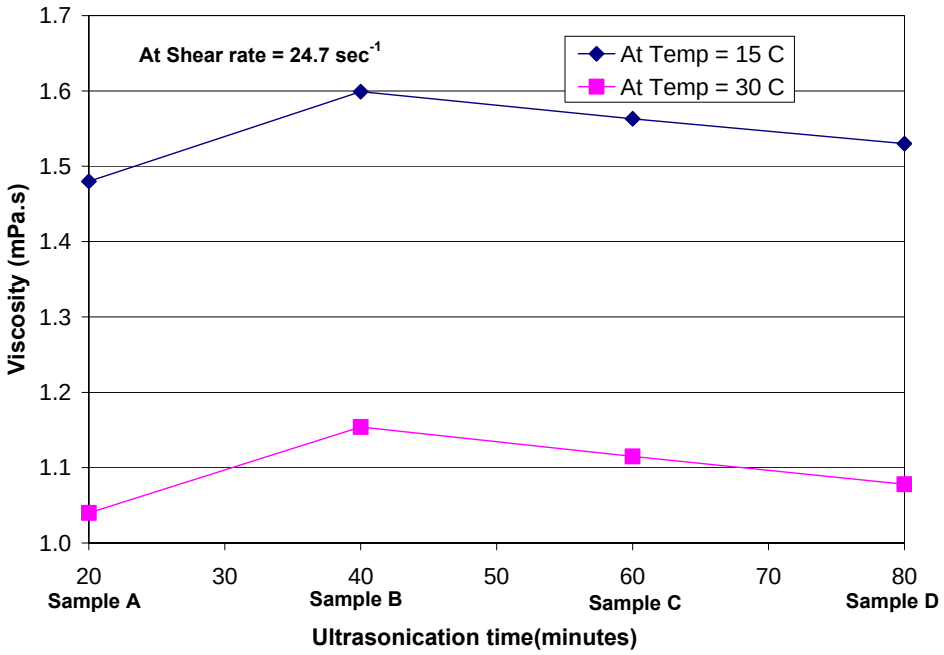

Fig. 21 Variation of viscosity with ultrasonication time.

Additionally, the viscosity trend with increase in ultrasonication time is shown in Fig. 21 at a shear rate of 24.7 sec^{-1}. From the figure, it is clear that the viscosity of the nanotube suspension first increased from sample A to sample B, and thereafter decreased with increase in ultrasonication time. The reason for the same can be explained as follows. According to Starr et al. [30], a clustered nanoparticle suspension is known to have a lower viscosity than a dispersed suspension. The viscosity increase in a dispersed sample is due to increased attractive surface interactions as a result of a greater surface-to-volume ratio [30].

For a fully dispersed sample, the growth in exposed nanoparticle surface with number of nanoparticles was much more than in a clustered sample, and hence greater viscosity was observed. In this work, it can be suggested that due to less dispersing energy in sample A, the nanotubes may not have received enough energy to overcome agglomerization and still remained in a clustered state. On the other hand, sample B has been sonicated for more time and has received enough energy to create a uniform dispersion which resulted in greater viscosity than sample A. After 40 minutes of sonication, it is seen that the viscosity continuously decreased with further sonication. The main effect in this regime is increased breakage of nanotubes with increase in ultrasonication time. The increased breakage rate reduces the lengths of nanotubes and hence the aspect ratio also decreases. It has been found by Yang et al. [31] that with increase ultrasonication of carbon nanotube-in-oil dispersions, the viscosity decreases. They explained this observation based on disruption of three-dimensional network of nanotubes with decrease in aspect ratios of nanotubes. This reasoning can also be confirmed by examining the wet-TEM pictures in Fig. 11-16.

From the presented data, a non-Newtonian behavior trend is seen; however, quantitative assessment requires a correlation between shear stress and shear rate. Therefore, plots for shear stress vs shear rates were made for each of the four samples including 0.25 wt % Gum Arabic. Curve-fitting was done for each of these plots and a mathematical relation was found to relate shear stress with shear rate. The mathematical relation obtained was compared with the viscosity models discussed in section 2.3, to find out

the flow behavior of the samples. See Fig. 22 for shear stress vs shear rate plot of 0.25 wt % Gum Arabic aqueous solution.

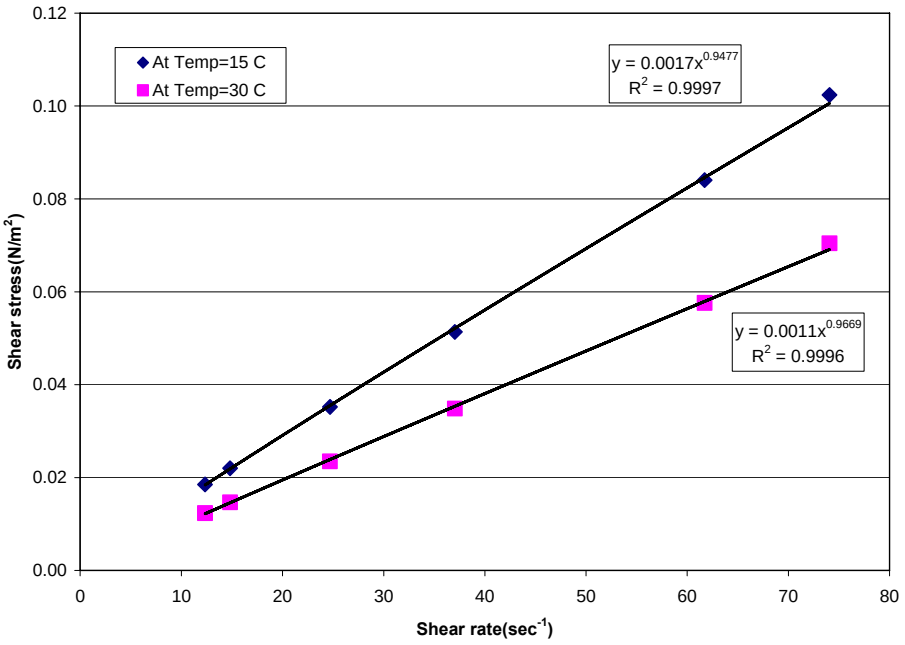

Fig. 22 Variation of shear stress with shear rate for 0.25 wt % Gum Arabic.

For similar plots for Sample A and B, see Fig. 23 and 24.

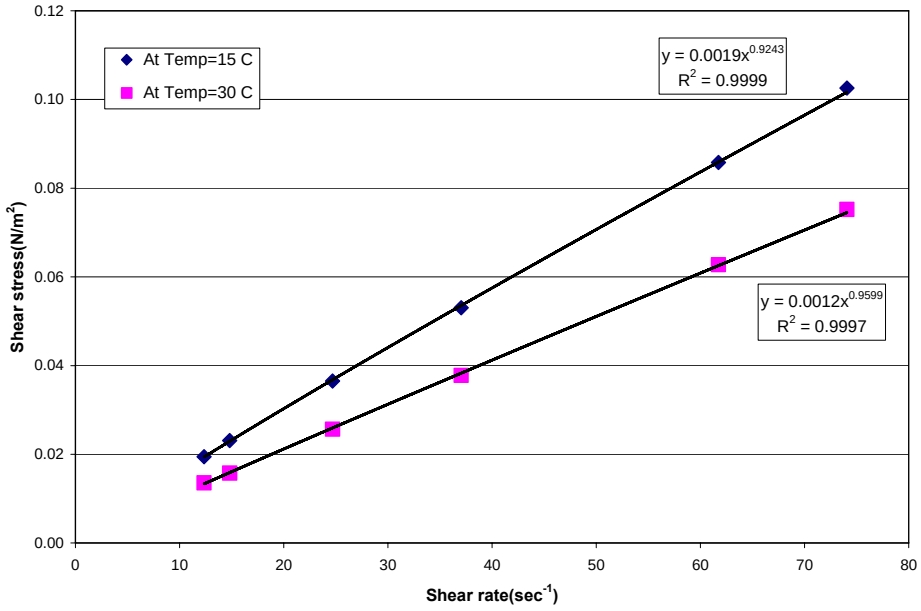

Fig. 23 Variation of shear stress with shear rate for Sample A. (1 wt % MWCNT, 0.25 wt % GA, 20 min sonication)

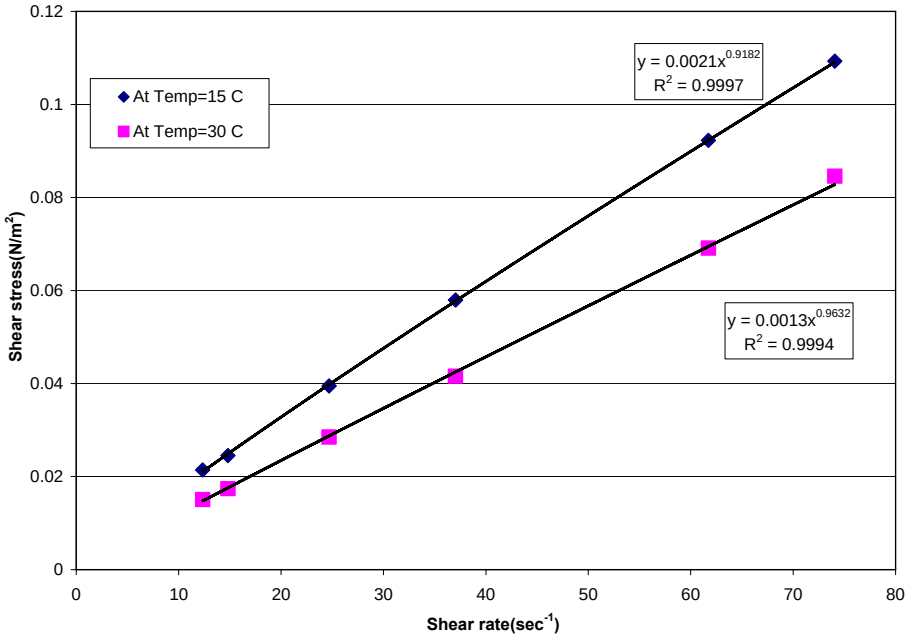

Fig. 24 Variation of shear stress with shear rate for Sample B. (1 wt % MWCNT, 0.25 wt % GA, 40 min sonication)

Similar plots are drawn for Sample C and D in Fig. 25 and 26.

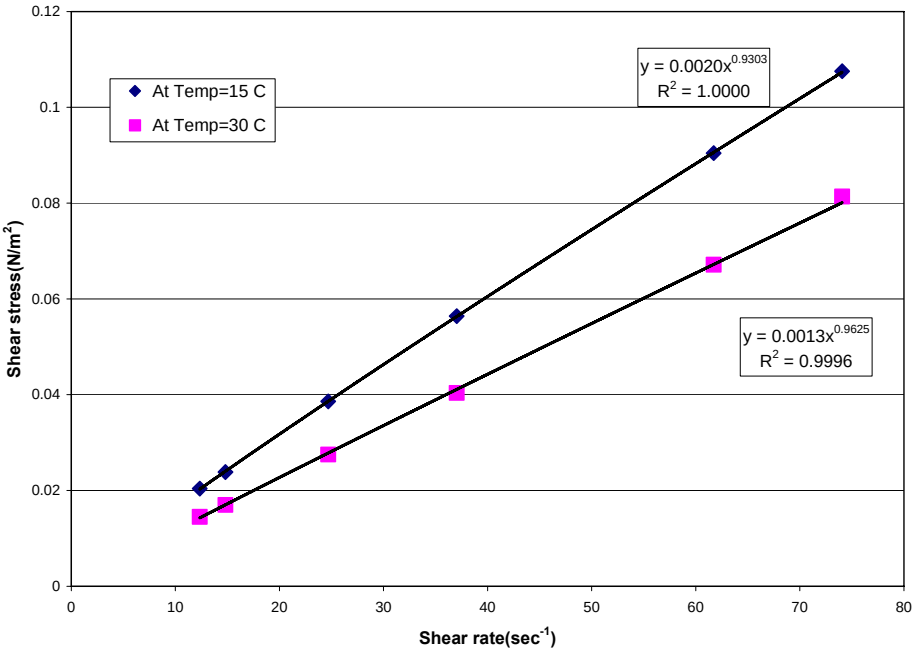

Fig. 25 Variation of shear stress with shear rate for Sample C. (1 wt % MWCNT, 0.25 wt % GA, 60 min sonication)

From the curve-fitting task, it was found that the nanofluid samples follow the Power Law ($\tau = K.\dot{\gamma}^n$) viscosity model. The R^2 value or correlation coefficient for each of the curves was found to be more than 0.999, thus indicating a good correlation. The unit of ' K ' is same as that of viscosity and therefore, it is indicative of a characteristic viscosity for a non-Newtonian fluid. The values for flow consistency index, K (mPa.s) and flow behavior index, n were found for each sample and 0.25 wt % GA at temperatures of 15 °C and 30 °C.

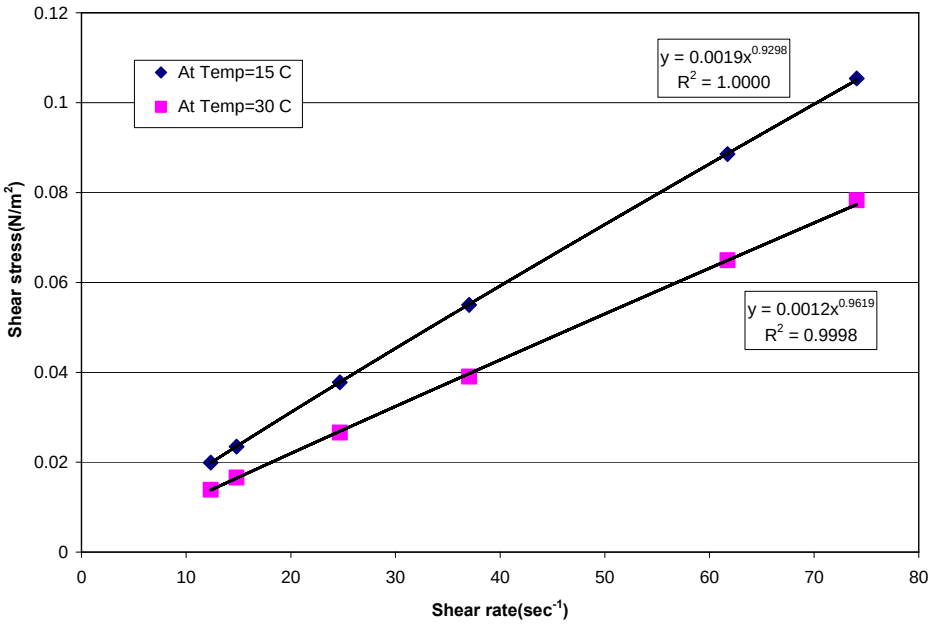

Fig. 26 Variation of shear stress with shear rate for Sample D. (1 wt % MWCNT, 0.25 wt % GA, 80 min sonication)

The flow consistency index has been plotted with respect to ultrasonication time in Fig. 27. From the figure, it is seen that as expected, the flow consistency index increases with the ultrasonication time from sample A to B and thereafter, it decreases. This is in agreement with the viscosity trend observed in Fig. 21. Additionally, the corresponding values for 0.25 wt % GA aqueous solution were found to be lower than the MWCNT nanofluid samples, thus indicating that it is less viscous. Additionally, the flow behavior index has been plotted with respect to ultrasonication time in Fig. 28. From the figure, it is seen that the flow behavior index at 30 °C, remains almost constant with ultrasonication time. However, the flow behavior index at 15 °C, first decreased and then increased. Since a low value of '*n*' indicates greater non-Newtonian behavior and a high

value indicates lesser non-Newtonian behavior, from the figure, it can be said that there is a greater degree of non-Newtonian behavior at lower temperatures in MWCNT nanofluid samples. However, at both the temperatures it is observed that 0.25 wt% GA aqueous solution has a higher value of flow behavior index, thus indicating that has a lesser degree of non-Newtonian behavior. Therefore, it can be said that the non-Newtonian behavior in MWCNT nanofluid samples is not just due to presence of Gum Arabic as shear-thinning effect has increased by addition of nanotubes.

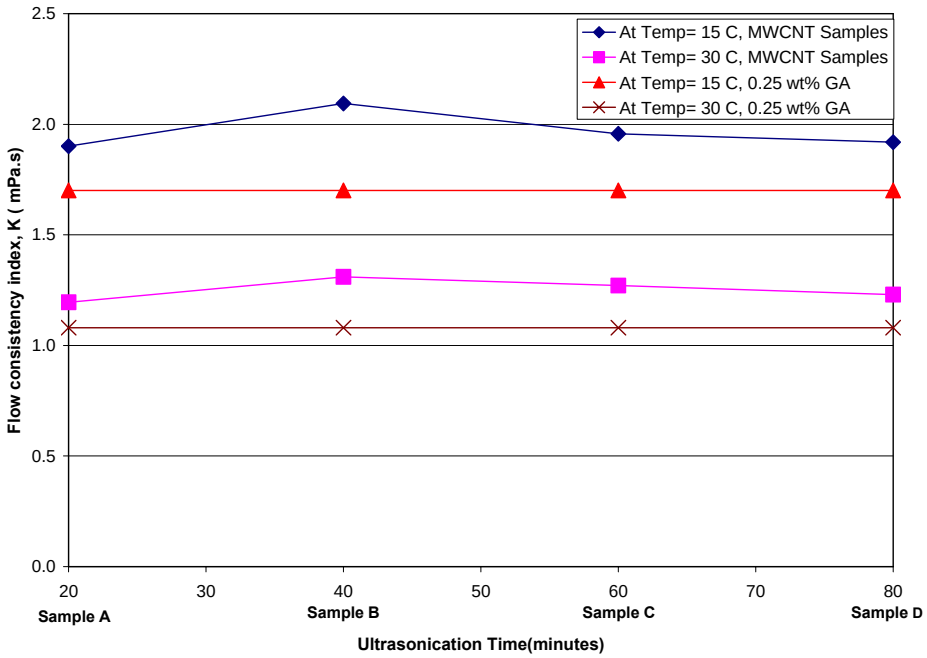

Fig. 27 Variation of flow consistency index with ultrasonication time.

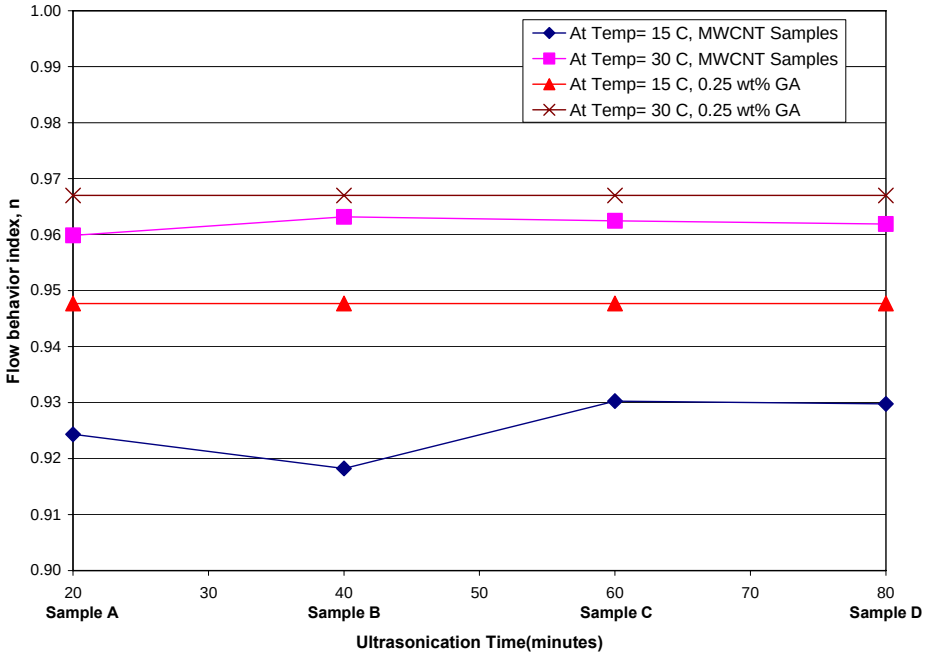

Fig. 28 Variation of flow behavior index with ultrasonication time.

4.3. Thermal conductivity data

Fig. 29 shows the absolute thermal conductivity data obtained using KD 2 Pro thermal properties analyzer. Measurements are taken for each of the four samples including DI water under different temperature conditions. Though the measured thermal conductivity of DI water was found to be slightly offset from the National Institute of Standards and Technology (NIST) thermal conductivity data, however, all the measurements for DI water were found to be within 2 % of the NIST values. The specified accuracy of the instruments was 5 %.

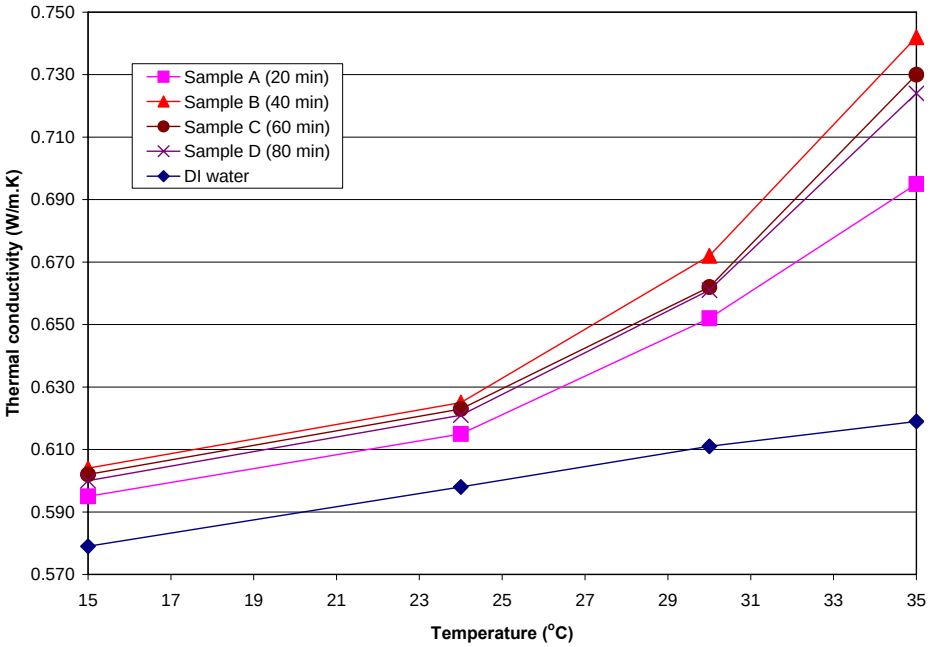

Fig. 29 Variation of thermal conductivity with temperature.

It was seen that unlike DI water, the thermal conductivity of the nanofluid samples, first increased slightly with temperature and after 24 °C, it increases non-linearly with temperature. One of the suggested reasons behind this phenomenon is the increased Brownian motion effect. Jang and Choi [26] suggested that as the temperature is increased, the viscosity of the nanofluid decreases, which results in increase in Brownian motion of nanoparticles, which sets convection-like effects resulting in enhanced thermal conductivity.

Fig. 30 shows this increase in terms of percentage enhancement with respect to the base fluid, DI water.

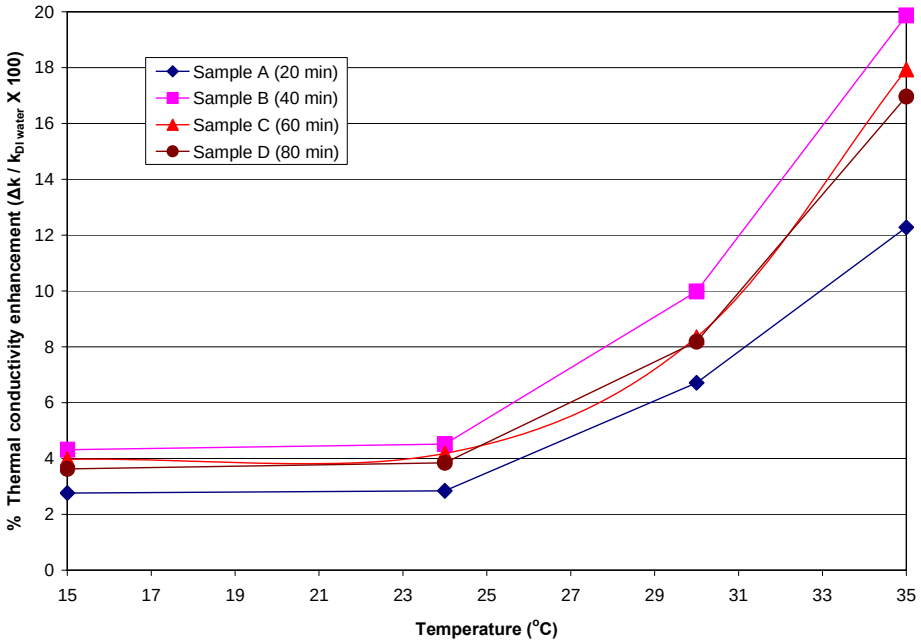

Fig. 30 Variation of percentage enhancement in thermal conductivity with temperature.

From the figure it can be seen, a maximum increase of 20% was obtained for Sample B at a temperature of 35 °C. The average density of MWCNT provided by the vendor was 2.1 gm/cm^3. Taking this value into account, a 1 wt % CNT suspension would be approximately 0.47 vol %.The percentage enhancement reported by Xie et al.[24] was 7% at 1 vol % MWCNT(aspect ratio ~ 2000) and that by Assael et al. [1] was 38% at 0.6 % vol MWCNT(aspect ratio ~ 500). Therefore, it can be said that both Xie el al. [24] and Assael et al. [1] used higher mass fractions of CNTs than in this work. However, the enhancement values obtained in this work are much better than the value obtained by Xie et al. [24], and slightly less than the value obtained by Assael et al [1]. However, Assael et al. [1] used a slightly higher volume fraction of MWCNT in his work which

could have resulted in better thermal conductivity value. However, the value reported by Ding et al. (i.e. 79% at 1 wt % MWCNT at 30 °C)[4] is much higher than the values obtained in this work even when the concentration of CNTs used in both the works is same. The exact reason for this discrepancy is unclear. It could be suggested that the reason could be related to the thermal and physical properties of the CNTs used in both works. Additionally, Ding et al. [4] did not specify the CNT aspect ratio, and it could be different from the aspect ratio (~50-2000) in this work.

Fig. 31 shows the thermal conductivity enhancement with respect to the ultrasonication processing. It can be seen that ultrasonication time increased the enhancement to a maximum value. Further processing reduced the enhancement.

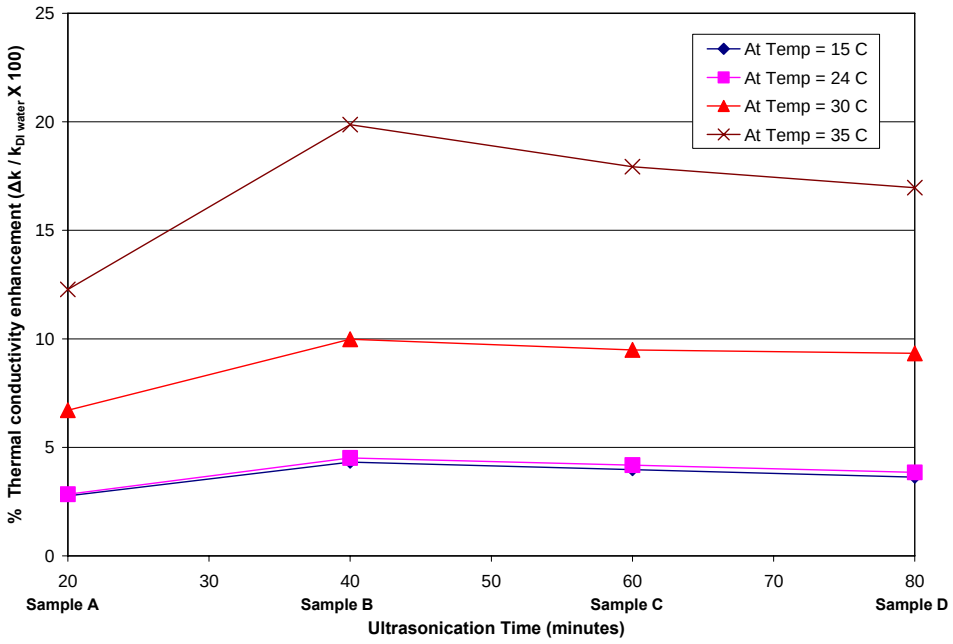

Fig. 31 Variation of percentage enhancement in thermal conductivity with ultrasonication time.

It is suggested that the reason for this phenomenon is associated with the aspect ratio of CNTs and the quality of three-dimension network established within each of the samples. It was found in section 4.1 from wet-TEM imaging that the aspect ratio of CNTs appears to have decreased with ultrasonication. This was particularly seen in Fig. 15 and 16 where Samples B and D were compared at 200 nm scale. Assael et al. [1] concluded that a decrease in aspect ratio decreases the thermal conductivity enhancement. Additionally, Wen and Ding [2] suggested the carbon nanotube networking as one of the factors contributing towards enhanced thermal conductivity as it provides avenues for ballistic energy transport. In Samples A to B, an increase in thermal conductivity enhancement was observed even though there was an increase in ultrasonication time. It can be said that in Sample A, the ultrasonication time was not enough to provide sufficient energy to facilitate preparation of a uniform dispersion. On the other hand, Sample B might have received sufficient energy for the creation of a uniform three-dimensional network of CNTs. Hence, it can be suggested that there was an optimum condition being established in Sample B, in context to aspect ratio and uniform three-dimensional network. On further ultrasonic processing, this condition got disturbed which resulted in decreased aspect ratio and decreased quality of three-dimensional network, and hence, a decrease in thermal conductivity enhancement. From Fig. 11-14, the quality of three-dimensional network can be seen.

4.4. Convective heat transfer data

A laminar flow, constant heat flux heat transfer section with multiple surface mount thermocouples was used for taking convective heat transfer measurements. The set-up was calibrated using DI water as test fluid and was calibrated to results within 5 % accuracy. The details of this procedure are mentioned in the Appendix B.

Once the set-up had been calibrated, measurements were taken for each of the four samples at three different flow rates including 40 mL/min, 60 mL/min and 80 mL/min. The heat flux conditions were maintained constant and near to 0.6 W/cm^2. However, the actual value of heat flux was calculated based on the heat added to the test fluid, using an energy balance equation. For the mentioned flow rates, the corresponding Reynolds numbers for DI water were found to be approximately 600, 900 and 1200, respectively. However, in case of CNT nanofluid as the viscosity of the samples changed appreciably with temperature and shear rate (due to non-Newtonian behavior), the Reynolds number for these samples was found to vary within a range of ± 100. Figures 32-34 show the variation of convective heat transfer coefficient for each of the four samples and DI water with respect to non-dimensionalized axial distance, x / D_i, from the inlet of the section at different Reynolds number. The figures also indicate the thermal entry length region and thermally fully developed region for DI water.

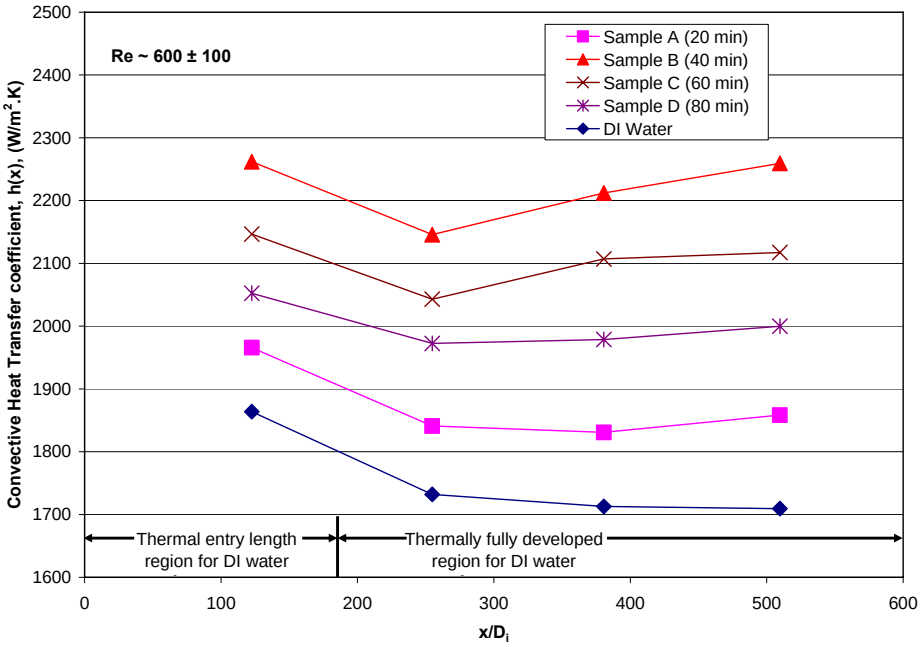

Fig. 32 Axial variation of heat transfer coefficient at Re ~ 600 ± 100.

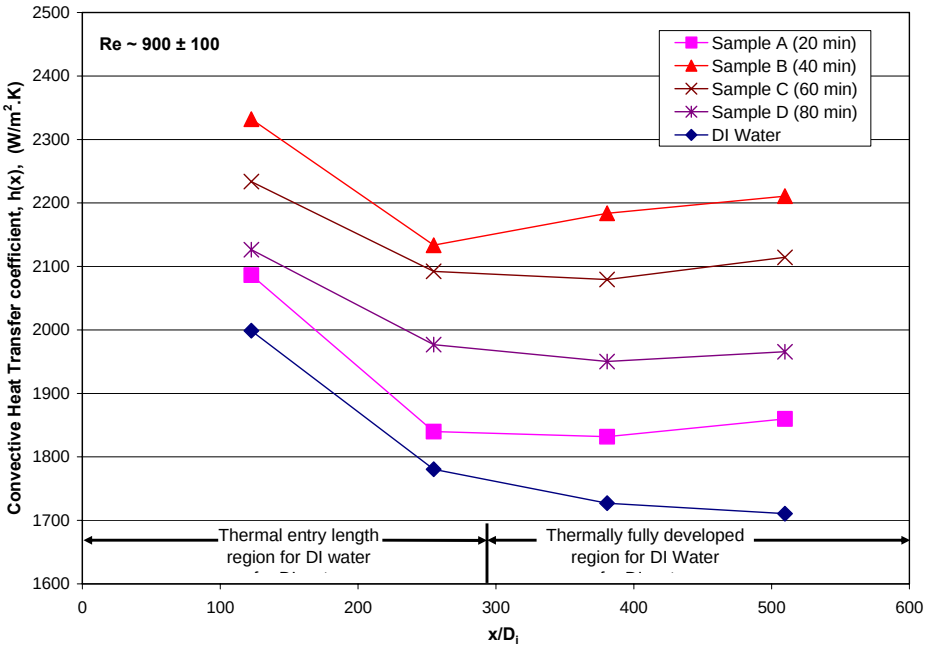

Fig. 33 Axial variation of heat transfer coefficient at Re ~ 900 ± 100.

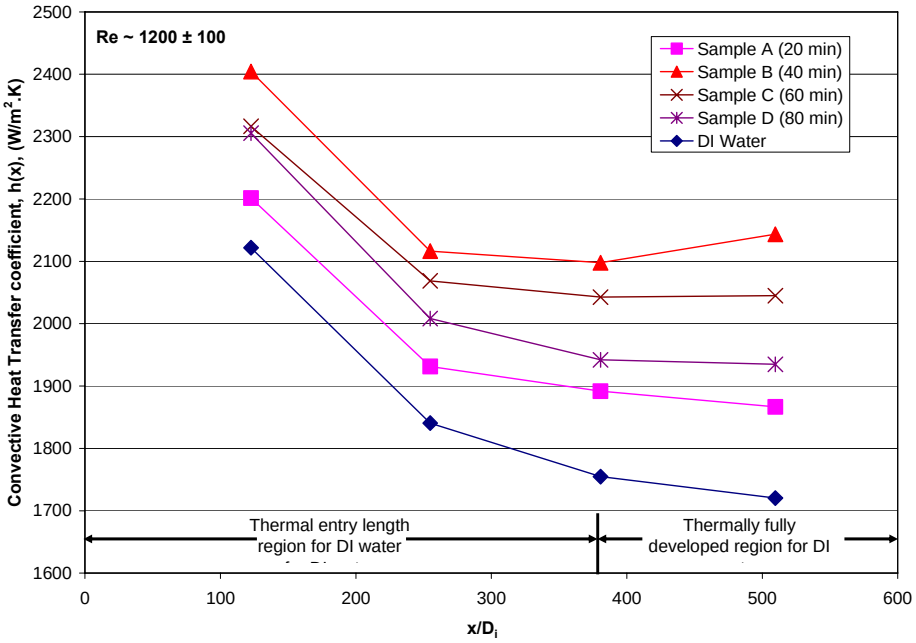

Fig. 34 Axial variation of heat transfer coefficient at Re ~ 1200 ± 100.

From Fig. 32-34, it can be seen that the laminar heat transfer coefficient decreases with axial distance. This is as expected due to entry length correction in a fully developed flow. For a pure Newtonian fluid flowing through a tube with circular cross section, the flow is hydrodynamically and thermally fully developed at $x/D_i \geq\sim (0.05\,\mathrm{Re})$ and $x/D_i \geq\sim (0.05.\mathrm{Re}.\mathrm{Pr})$, respectively. Once the flow has become fully developed, the heat transfer coefficient value stabilizes for pure fluids. A similar trend is observed for CNT nanofluid samples up to a certain extent.

A clear enhancement in heat transfer coefficient was observed in case of CNT nanofluid samples as compared to DI water. The extent of the enhancement can be seen in Fig. 35-37.

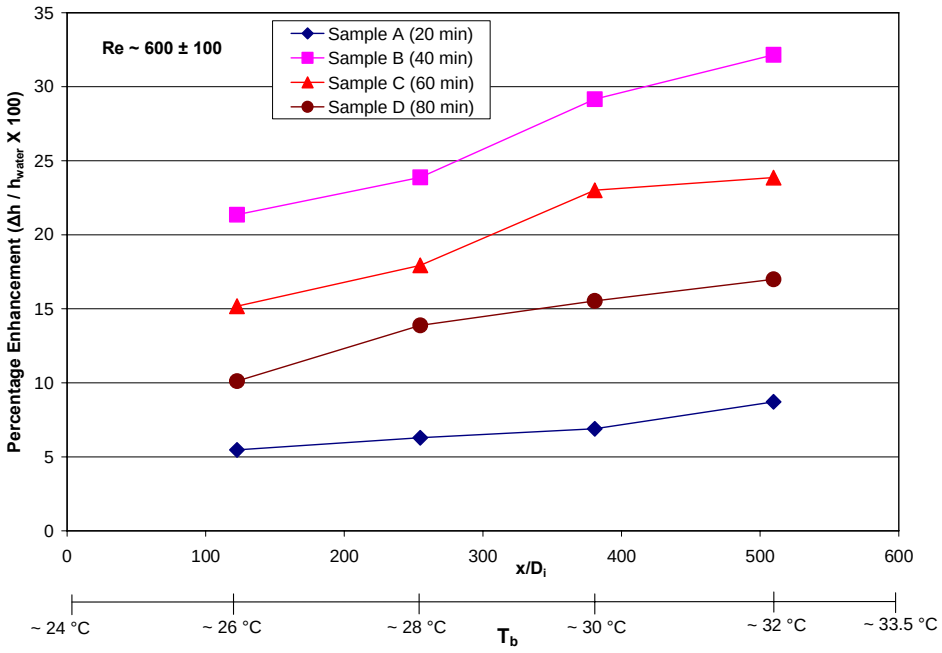

Fig. 35 Enhancement in heat transfer with axial distance and bulk temperature at Re ~ 600 ± 100.

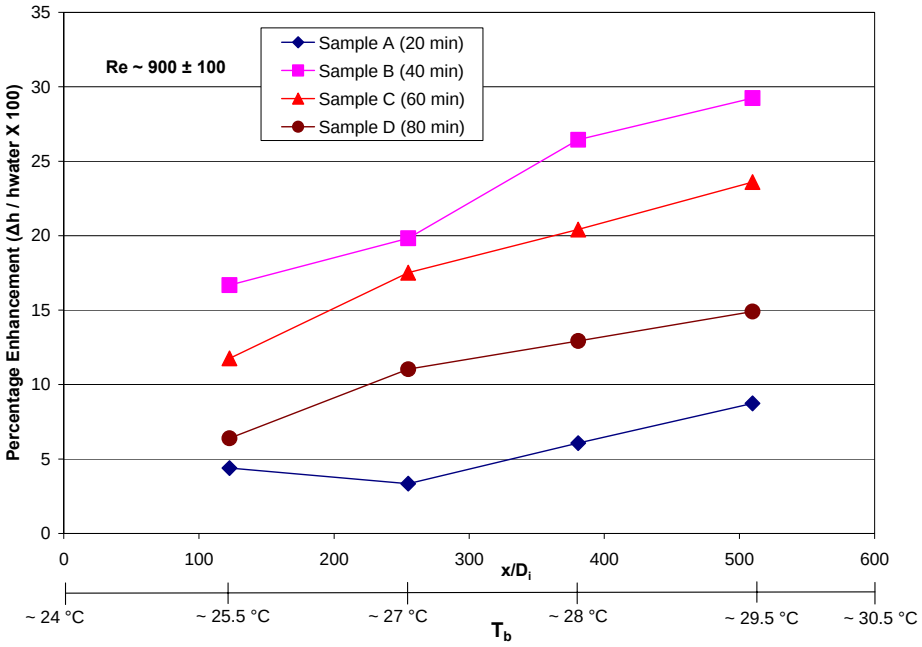

Fig. 36 Enhancement in heat transfer with axial distance and bulk temperature at Re ~ 900 ± 100.

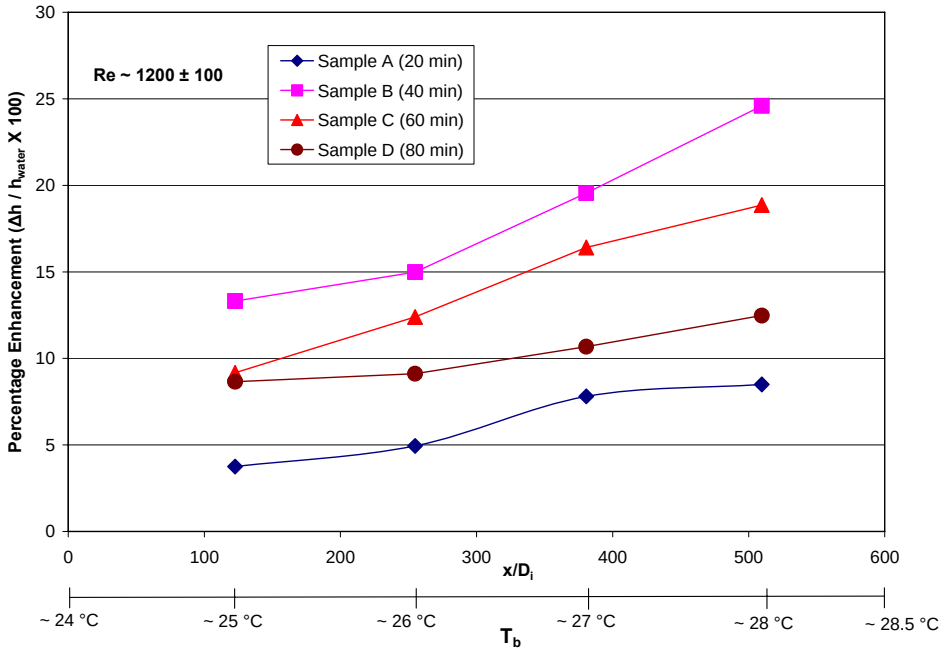

Fig. 37 Enhancement in heat transfer with axial distance and bulk temperature at Re ~ 1200 ± 100.

It can be seen from Fig. 35-37, that the percentage enhancement in convective heat transfer coefficient increases continuously with the axial distance with the maximum increase found to be 32 % for Sample B at Re ~ 600 ± 100. This increase is more than the maximum increase of 20 % in thermal conductivity observed in Sample B. These observations were found to both agree and disagree with the previous work for nanofluids. Ding et al.[4] reported similar trends where much more dramatic increase in heat transfer coefficient enhancement (i.e. 375 % at 0.5 wt % CNT) as compared to thermal conductivity enhancement (i.e. 37 % at 0.5 wt % CNT) were observed. Similar trends were reported by Wen and Ding [22], and Xuan and Li [23]. Wen and Ding [22] reported a heat transfer coefficient enhancement of 47 %, and thermal conductivity enhancement of 10 % at 1.6 vol % Al_2O_3 spherical nanoparticles in DI water. Xuan and Li [23] reported a heat transfer coefficient enhancement of 60 %, and thermal conductivity enhancement of 12.5 % at 2 vol % Cu spherical nanoparticles. In this work, in a similar way, the heat transfer coefficient enhancement has been found to be more than thermal conductivity enhancement. Ding et al. [4] provided several possible reasons for this observation. From convective heat transfer fundamentals, the heat transfer coefficient, h can be approximately represented as k / δ_t where k and δ_t are the thermal conductivity of the test fluid and thickness of thermal boundary layer, respectively. For a fluid with Pr = 1, the 'h'can be approximately given by k / δ where δ is the hydrodynamic boundary layer thickness. Water is known to have a Pr ~ 2-14. In our case, the Pr of the samples was found between 4 to 6. With increase in 'k'and

decrease in δ_t or δ, the value of h should increase. It has been found that the addition of CNTs enhances the thermal conductivity of water; however, this enhancement is less than the heat transfer enhancement. A simultaneous decrease in δ or δ_t could be suggested as the one reason for the observed heat transfer enhancement. This could be explained by possible boundary layer thinning effect most likely caused by CNTs in the fluid. Additionally, it has been found previously by Sohn and Chen [32] that for a liquid comprising of solid particles, thermal conductivity enhancements under shear conditions are greater than those observed under static conditions. This phenomenon was attributed to microconvective effects due to presence of an eddy scale convection mechanism. Significant enhancements were seen in his work for samples having Peclet number greater than 300, where Peclet number, Pe is defined as $\frac{\bar{\dot{\gamma}}_f .d_p^2}{\alpha_f}$ where $\bar{\dot{\gamma}}_f, d_p$ and α_f are local mean shear rate experienced by fluid, particle diameter and thermal diffusivity of the fluid, respectively. From calculations as described in Appendix C, we obtained that for the Peclet number to be at least 300, the particle size should be at least 230 μm at Re ~ 600 ± 100 at 30 °C. Though individual nanotube is much smaller than 230 μm, however, as observed from wet-TEM pictures, CNTs form networks in dispersion and hence, the effective particle size could be much higher than 230 μm. This could be another possible contributing factor in explaining the considerably higher heat transfer enhancement when compared to the thermal conductivity values under static conditions. Also, CNTs in the nanofluid could experience a re-arrangement effect due to non-uniform shear rate in the radial direction in the tube. This could lead to a non-uniform

viscosity and thermal conductivity. Wen and Ding [33] showed previously that such a change could result in a high Nusselt number and hence, a higher heat transfer coefficient. Finally, thermal convection is improved if the viscosity near the wall of a flowing in a tube is decreased with respect to the viscosity of the bulk fluid [34]. In case of flow inside a tube, the temperatures at the wall and the centerline are maximum and minimum, respectively. Due to these temperature variations, there are additional variations in viscosity of the fluid in the radial direction, resulting in minimum viscosity at the wall and maximum viscosity at the centerline. This leads to convective effects in the radial direction, and hence, improved heat transfer coefficient [34].

Ding et al. [4] observed that the percentage enhancement of heat transfer coefficient increased up to a certain value of x/D_i and after that it decreased with x/D_i. However, in this work, we have found that the percentage enhancement increases continuously with the axial distance. One of the suggested reasons for this phenomenon could be an increase in thermal conductivity with axial distance. This is can be explained as follows. It has been observed in this work that thermal conductivity of the CNT nanofluids increased significantly with temperature. The bulk temperature of the CNT nanofluid increases with axial distance (Eq. 3.8., Fig. 35-37), which results in an increase in the thermal conductivity of the CNT nanofluid with axial distance. As the heat transfer coefficient of a fluid is directly proportional to the thermal conductivity (Eq. 3.10), this in turn results in slight increase in heat transfer coefficient.

In addition to measuring the heat transfer coefficient, the local Nusselt number was calculated for each sample to determine the net heat transfer enhancement in a non-dimensionalized way using Eq. 3.11 ($Nu(x)= h(x). D_i / k$). The corresponding thermal conductivity values for CNT samples were calculated by linear interpolation from Fig. 29 after considering the bulk temperature from Fig. 35. These are plotted for Re ~ 600 ± 100 in Fig. 38 to show a typical behavior. It was found that the experimental Nusselt number in case of DI water matched well with theoretical fully-developed Nusselt number value of 4.36 for a constant heat flux case. Further, from the Nusselt number of each CNT sample, a clear enhancement can be seen.

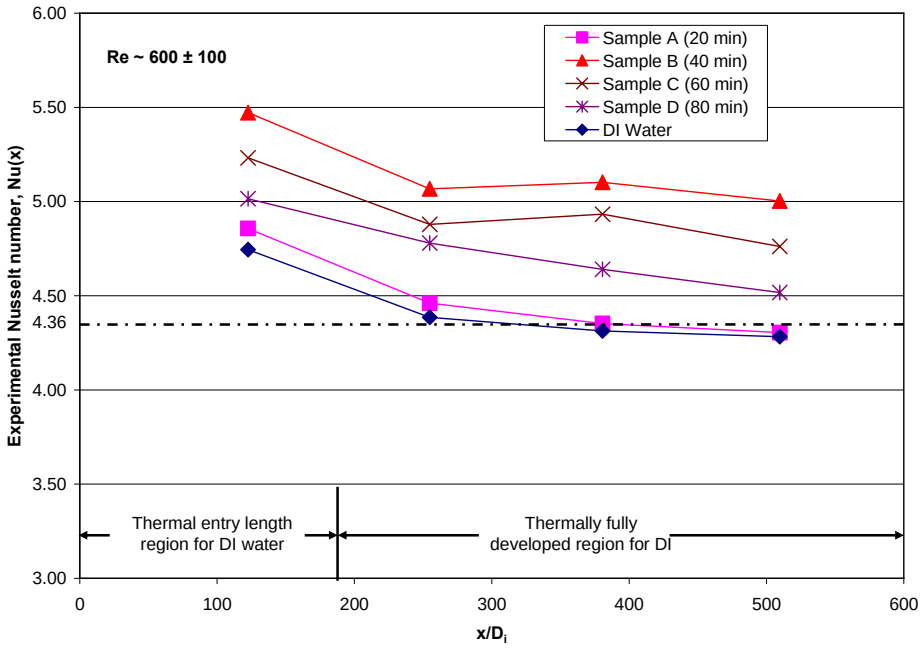

Fig. 38 Variation of experimental Nusselt number with axial dstance at Re ~ 600±100.

Variations for heat transfer coefficient enhancement with Reynolds number are shown in Fig. 39 and 40 for Sample A and B, respectively. It can be seen from these figures that for the same sample, the heat transfer enhancement slightly decreases with increase in Reynolds number. This is can be possibly explained by decrease in bulk temperature of nanofluid, at a particular x/D_i value with increase in Reynolds number (Fig. 35-37). It was previously seen that the thermal conductivity enhancement has considerable dependence on the bulk temperature of the nanofluid. Therefore, due to decrease in bulk temperature of the nanofluid, its thermal conductivity enhancement also decreases. This results in slight decrease in heat transfer enhancement. However, as this enhancement decrease was found to be slight, further investigation is required to arrive at a conclusion. Similar trends are seen for Sample C and D in Fig. 41 and 42, respectively.

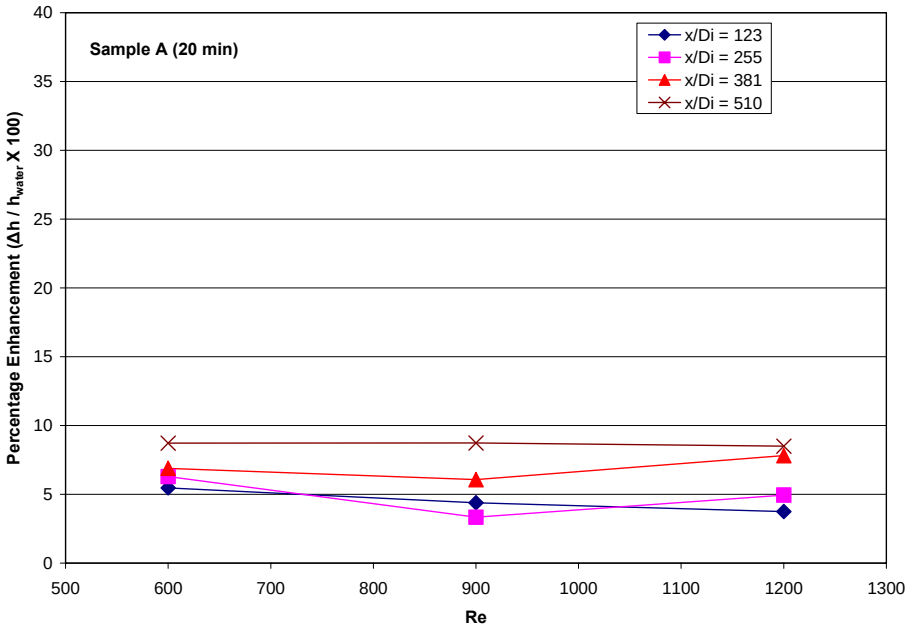

Fig. 39 Variation in heat transfer coefficient enhancement with Reynolds number for Sample A.

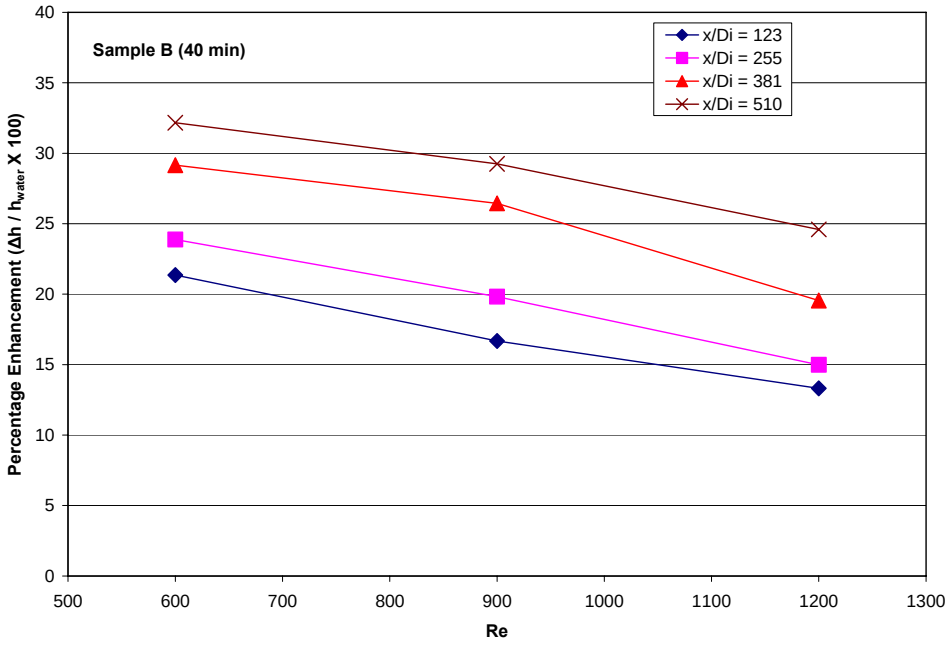

Fig. 40 Variation in heat transfer coefficient enhancement with Reynolds number for Sample B.

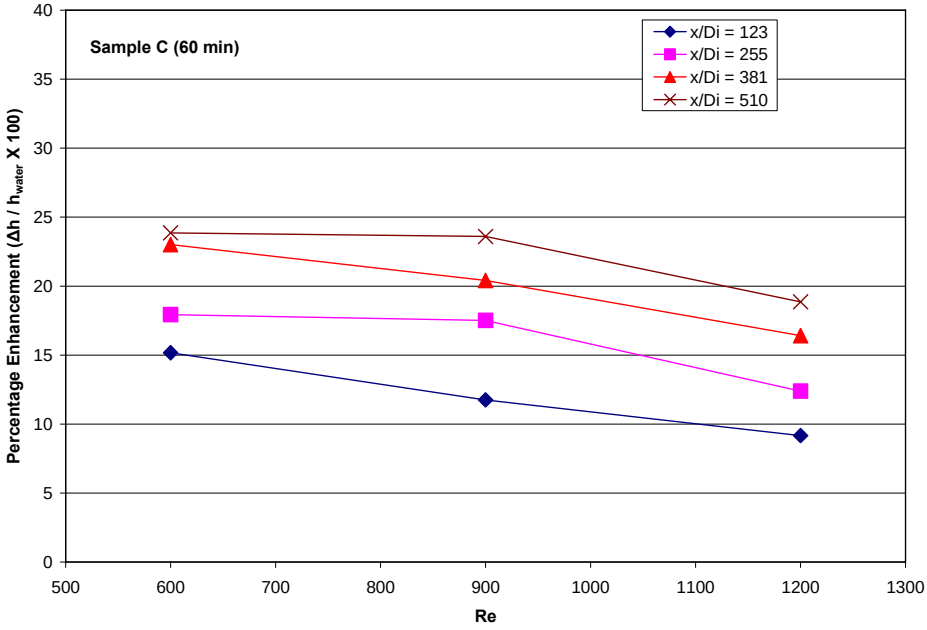

Fig. 41 Variation in heat transfer coefficient enhancement with Reynolds number for Sample C.

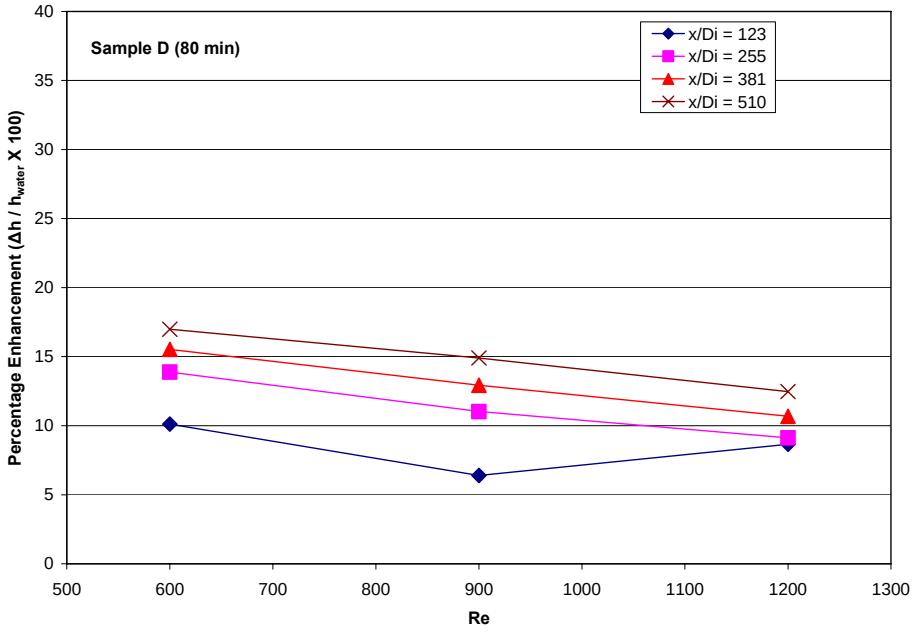

Fig. 42 Variation in heat transfer coefficient enhancement with Reynolds number for Sample D.

Figures 43 and 44 show the variation of heat transfer coefficient enhancement with ultrasonication time at Re ~ 600 ± 100 and Re ~ 900 ± 100, respectively.

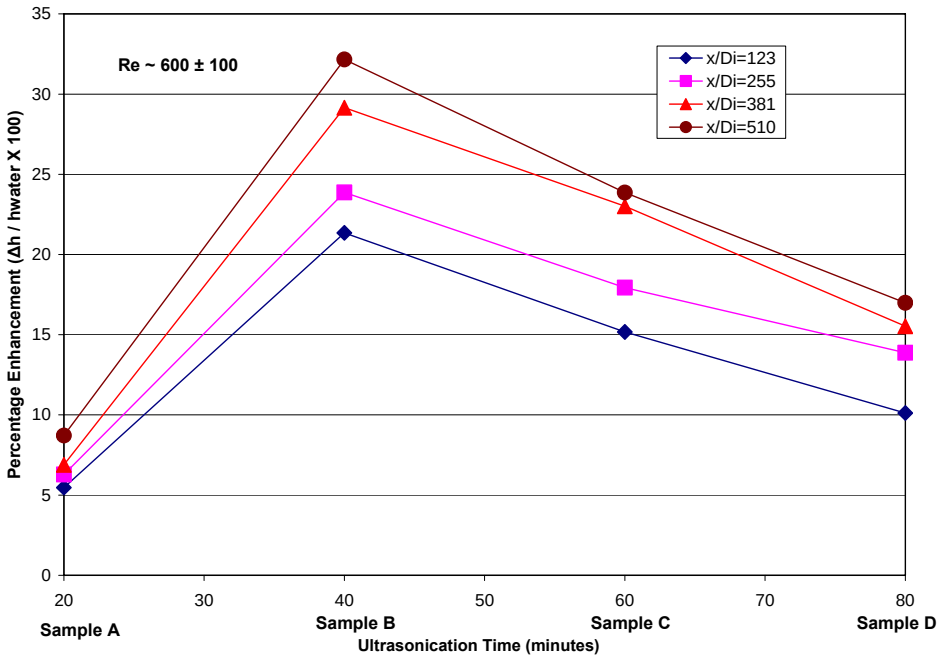

Fig. 43 Variation of heat transfer coefficient enhancement with ultrasonication time at Re ~ 600 ± 100.

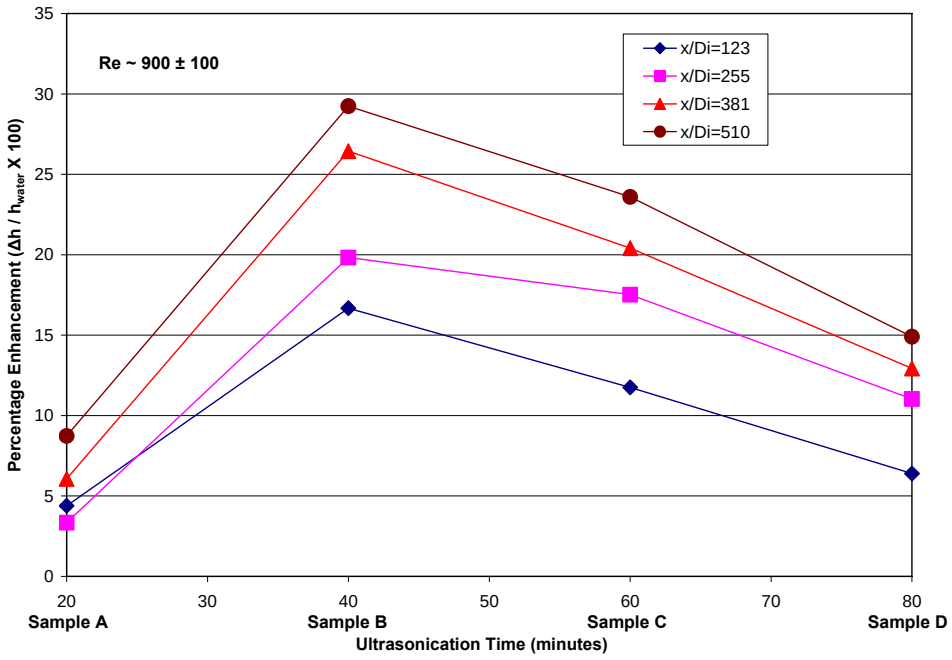

Fig. 44 Variation of heat transfer coefficient enhancement with ultrasonication time at Re ~ 900 ± 100.

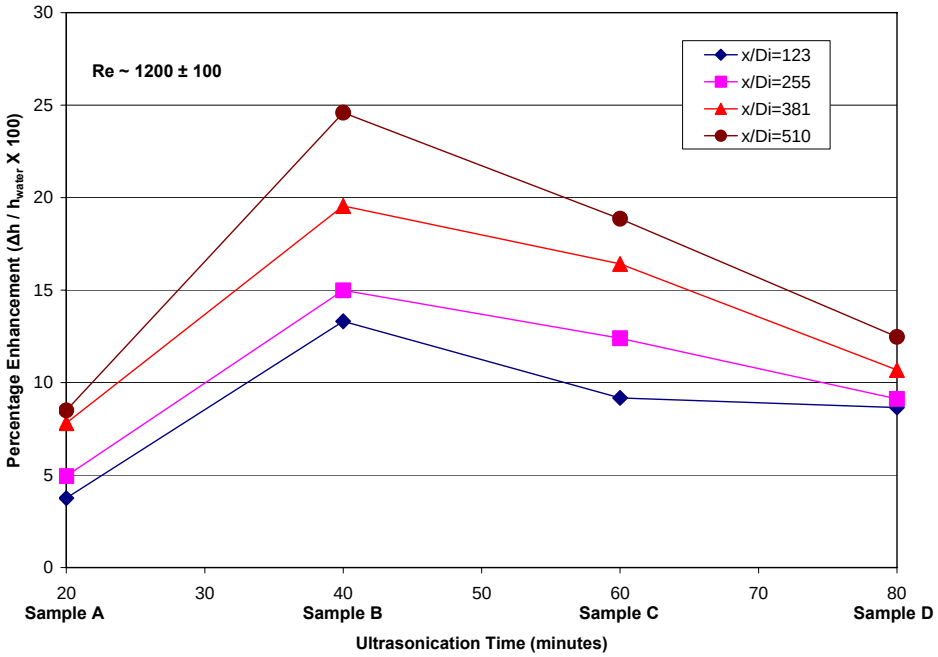

Fig. 45 Variation of heat transfer coefficient enhancement with ultrasonication time at Re ~ 1200 ± 100.

Similar plot is shown in Fig. 45 for Re ~ 1200 ± 100. From Fig. 43-45, it is seen that the heat transfer coefficient enhancement increases with ultrasonication processing time until a certain maximum and then it starts decreasing. This phenomenon is observed at all the three Reynolds number. A similar trend was seen in the thermal conductivity data. Therefore, it can be said that the thermal conductivity does has some effect on heat transfer performance as well. The reason for the phenomenon could be again associated with the aspect ratio of CNTs and the quality of three-dimension network established within each of the samples, as described in section 4.3.

Additionally, calculations were done to find Prandtl number (Pr) for Sample B at 15 °C and 30 °C. As sample B showed a non-Newtonian behavior, viscosity values were found from power law correlations found in section 4.2 at temperatures of 15 °C and 30 °C. The mean shear rate, $\dot{\gamma}$ used for the calculation was 911.75 sec^{-1} which corresponded to Re ~ 600 ± 100 as described in Appendix C. The ratio of Prandtl numbers was calculated for Sample B with respect to water at the both the temperature conditions. The ratio is defined as $\frac{\mathrm{Pr}_{NF}}{\mathrm{Pr}_{water}} = \frac{\mu_{NF}}{\mu_w}.\frac{k_w}{k_{NF}}$ assuming changes in specific heat, c_p to be negligible since in the presence of only 1 wt % of MWCNT. The thermal conductivity values were taken from the experimental data at 15 °C and 30 °C. It was found that this ratio decreased with increasing temperature as shown in Fig. 46. It was seen that that bulk temperature of a fluid continuously increased along the axial distance in flow direction. Hence, it could be said that the Prandtl number ratios decrease along the length of the heat transfer section. This phenomenon could give further insight in explaining heat transfer enhancement in MWCNT nanofluids. Future work in this direction could provide a more comprehensive insight in explaining heat transfer mechanisms in nanofluids.

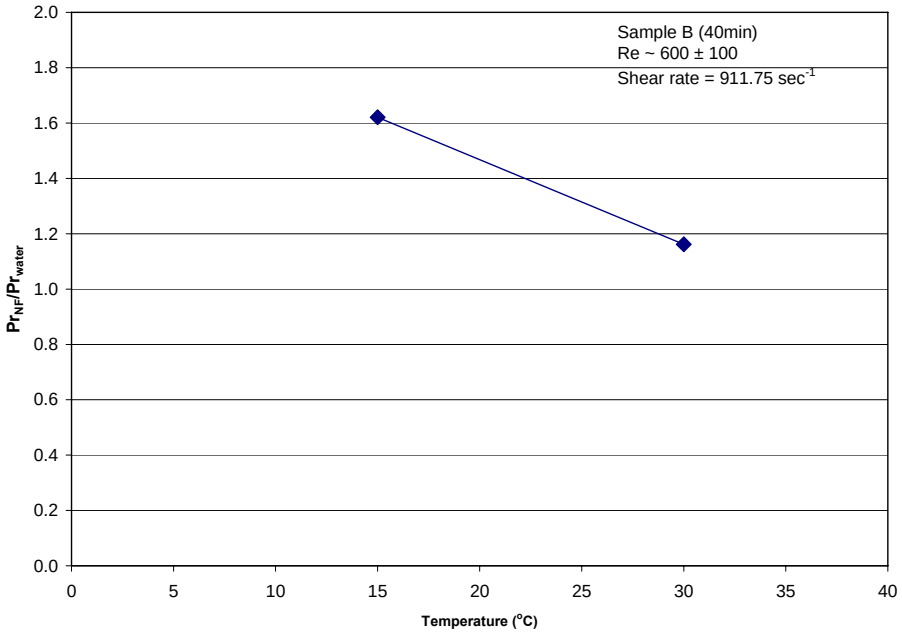

Fig. 46 Variation of Prandtl number ratios of nanofluid and water with temperature.

CHAPTER V

CONCLUSIONS

Through this work, it has been shown that CNT nanofluids can be used as heat transfer fluids. However, the preparation method of the nanofluids is an important step affecting the overall heat transfer performance. It was found that at a given CNT composition, there are certain optimum processing conditions (ultrasonication time in this case) which give the maximum enhancement in the heat transfer performance.

The chapter presents the conclusions drawn from the results obtained from imaging, viscosity, thermal conductivity and convective heat transfer measurements. Additionally, recommendations for future work in the area are provided.

5.1. Imaging conclusions

From the wet-TEM imaging of the CNT samples, it can be said that:

- The dispersing energy or ultrasonication has two-fold effect on the CNT nanofluids. Below the optimum processing time, the ultrasonication aids in forming better dispersions, however, once the optimum time has been reached further ultrasonication results in increased breakage rate of the nanotubes, and hence reduces the aspect ratio of CNTs. The optimum ultrasonciation time was

found to be 40 minutes at 1 wt % MWCNT concentration, 20 kHz frequency and energy density of 113 J/g.

- Reduction in the aspect ratio of the CNTs affects the quality of the three dimensional network formed within the nanotubes in the dispersion.

5.2. Viscosity conclusions

From the viscosity data, it can be said that:

- CNT nanofluids exhibit a shear-thinning (psuedoplastic) non-Newtonian behavior. This effect is due to deagglomeration of CNTs bundles with increase in shear rate, as seen in other non-Newtonian fluids

- Additionally, viscosity of the nanofluids increases with sonication time until a maximum value is reached and decreases thereafter. The viscosity increased until 40 minutes but thereafter, it decreased on further sonication. The initial increase can be explained by declustering of CNT bundles, resulting in formation of a better dispersion. The later decrease in viscosity can be explained by increased breakage rate of CNTs, resulting in shorter nanotubes, and hence, inferior networking of CNTs in dispersion.

- Addition of CNTs does not affect the viscosity dependence on temperature and the suspension showed similar behavior as the base fluid. All the samples were found to have reduced viscosity at elevated temperature.

- CNT nanofluids follow the Power Law viscosity model. The flow consistency index was found to be higher than that of 0.25 wt % Gum Arabic aqueous solution. Also, the flow behavior index was found to be lower than that of 0.25 wt % Gum Arabic aqueous solution. This shows the non-Newtonian character in CNT nanofluids could not be solely attributed to the presence of Gum Arabic.

5.3. Thermal conductivity conclusions

From the thermal conductivity data, it can be said that:

- The percentage enhancement in thermal conductivity of CNT nanofluids increases considerably after 24 ^{o}C. This could be explained by a lower viscosity at elevated temperature, resulting in an expected increase in Brownian motion and hence, an increase in thermal conductivity.

- The maximum percentage enhancement in thermal conductivity was 20 %, and was observed in Sample B which was sonicated for 40 minutes.

- Additionally, for a given composition, maximum thermal conductivity enhancement is obtained under certain optimum processing conditions. The thermal conductivity enhancement increased until the ultrasonication time of 40 minutes and was found to decrease with further sonication. The initial increase was explained by formation of better three-dimensional network in the CNT samples and the later decrease was explained by decrease in aspect ratio of CNTs. From the wet-TEM pictures, similar phenomenon was observed where aspect ratio and CNT network were found to be deteriorated in Sample D.

5.4. Convective heat transfer conclusions

From the convective heat transfer measurements, it can be said that:

- The heat transfer coefficient of CNT nanofluids decreases with axial distance in the test section until it reaches an almost steady value. This is due to entry length phenomenon in internally forced convection.

- The maximum percentage enhancement in heat transfer coefficient was 32 % at Re ~ 600 ± 100 and was observed in Sample B which was sonicated for 40 minutes.

- The percentage enhancement in heat transfer coefficient at a particular axial distance in the test section was found to slightly decrease with increase in Reynolds number. This effect was possibly attributed to the decrease in thermal conductivity enhancement with decrease in bulk temperature with increase in Reynolds number. However, further investigation is required to arrive at the exact reason.

- The maximum percentage enhancement in heat transfer coefficient (i.e. 32 %) was found to be more than the maximum percentage enhancement in thermal conductivity (i.e. 20 %). Many possible reasons could be suggested for this phenomenon. Firstly, a decrease in boundary layer thickness due to presence of CNTs. Secondly, a further enhanced thermal conductivity under dynamic conditions leading to microconvective effects in the fluid. Additionally, possibility of particle- rearrangement occurring in the fluid due to non-uniform shear conditions in the radial direction which lead to a non-uniformity in viscosity (due to shear thinning behavior) and thermal conductivity. This could lead to an improved Nusselt number. Finally, due to temperature variations in radial direction, viscosity variations induce convective effects which improve heat transfer.

- The percentage enhancement in heat transfer coefficient was found to continuously increase with the axial distance in the test section. The reason

behind the phenomenon is explained by the contribution from a considerable increase in thermal conductivity with increase in bulk temperature with the axial distance.

- Finally, a trend similar to thermal conductivity enhancement with ultrasonication time was found in heat transfer data too. This could be once again explained by the optimum processing time which gives a good balance between aspect ratio and quality of three-dimensional network.

5.5. Recommendations for future work

Though from experimental work, it is known that nanofluids exhibit enhanced heat transfer performance but the extent of contribution by each proposed physical mechanism behind this phenomenon is still unknown. Simultaneous computer simulation work in the area which takes into account the non-Newtonian characteristic of the nanofluids could give a better understanding in the area.

From theory, it is known that single walled carbon nanotubes (SWCNT) have a higher thermal conductivity than multi-walled carbon nanotubes (MWCNT) [9,10]. Therefore, theoretically SWCNT have a higher potential of heat transfer improvement. However, no work has been reported using SWCNT. The reasons for these are cost of SWCNTs which is high, and the fact that it is difficult to decluster the SWCNT bundles in

dispersions. An experimental work in this direction could open new avenues in nanofluid research.

Additionally, effect of various other parameters like the base fluid (ethylene glycol, mineral oil, refrigerants), aspect ratio, flow conditions (laminar, transition, turbulent) is an area which could provide further understanding of CNT based heat transfer fluids.

Finally, presently the experimental data previously reported for nanofluid research has large variations. This is due to lack of standardized procedures for preparing nanofluids. An extensive work in this area could help in future research activities as well as supporting commercialization efforts in the area of nanofluids for heat transfer applications.

REFERENCES

[1] Assael, M.J., Chen, C.F., Metaxa, I. and Wakeham, W.A., 2004, "Thermal Conductivity of Suspensions of Carbon Nanotubes in Water," International Journal of Thermophysics, **25**(4), pp. 971-985.

[2] Wen, D. and Ding, Y., 2004, "Effective Thermal Conductivity of Aqueous Suspensions of Carbon Nanotubes (Carbon Nanotube Nanofluids)," Journal of Thermophysics and Heat Transfer, **18**(4), pp. 481-485.

[3] Assael, M.J., Metaxa, I., Arvanitidis,J., Christofilos, D. and Lioustas, C., 2005, "Thermal Conductivity Enhancement in Aqueous Suspensions of Carbon Multi-Walled and Double-Walled Nanotubes in the Presence of Two Different Dispersants," International Journal of Thermophysics, **26**(3), pp. 647-664.

[4] Ding, Y., Alias, H., Wen, D. and Williams, R.A., 2006, "Heat transfer of Aqueous Suspensions of Carbon Nanotubes (CNT nanofluids)," International Journal of Heat and Mass Transfer, **49**, pp. 240-250.

[5] Choi, S. U. S., Zhang, Z. G., Yu, W., Lockwood, F. E. and Grulke, E. A., 2001, "Anomalous Thermal Conductivity Enhancement in Nanotube Suspensions," Applied Physics Letters, **79**(14), pp. 2252-2254.

[6] Faulkner, D.J., Rector, D.R., Davidson, J. and Shekarriz, R., 2004, "Enhanced Heat Transfer through the use of Nanofluids in Forced Convection," *Proceedings of IMECE*, Anaheim, CA, pp. 1-6.

[7] Iijima, S., 1991, "Helical Microtubules of Graphitic Carbon," Nature, **354**, pp. 56-58.

[8] Iijima, S. and Ichihashi, T., 1993, "Single-shell Carbon Nanotubes of 1-nm Diameter," Nature, **363**, pp. 603-605.

[9] Martel, R., Derycke, V., Lavoie, C., Appenzellar, J., Chan, K.K., Tersoff, J. and Avouris, P., 2001, "Ambipolar Electrical Transport in Semiconducting Single-Wall Carbon Nanotubes," Physical Review Letters **87** (25), pp. 256805-1-4.

[10] Kim, P., Shi, L., Majumdar, A., and McEuen, P. L., 2001, "Thermal Transport Measurements of Individual Multiwalled Nanotubes," Physical Review Letters, **87**(21), pp. 215502-1–4.

[11] Berber, S., Kwon, Y.K., and Tomanek, D., 2000, "Unusually High Thermal Conductivity of Carbon Nanotubes," Physical Review Letters, **84**(20), pp. 4613–4616.

[12] Hilding, J., Grulke, E.A., Zhang, Z.G. and Lockwood, F., 2003, "Dispersion of Carbon Nanotubes in Liquids," Journal of Dispersion Science and Technology, **24**(1), pp. 1-41.

[13] Hamilton, R.L. and Crosser, O.K., 1962, "Thermal Conductivity of Heterogeneous Two-Component Systems," IEC Fundamentals, **1**(3), pp. 187-191.

[14] Hunter, R.J., 1986, *Foundations of Colloid Science*, Oxford University Press, New York.

[15] Bandyopadhyaya, R., Nativ-Roth, E., Regev, O., Rozen, R.Y., 2002, "Stabilization of Individual Carbon Nanotubes in Aqueous Solutions," Nano Letters, **2**(1), pp. 25-28.

[16] Pak, B.C. and Cho, Y.I., 1998, "Hydrodynamic and Heat Transfer Study of Dispersed Fluids with Submicron Metallic Oxide Particles," Experimental Heat Transfer, **11**(2), pp. 151-170.

[17] Das, S.K, Putra, N. and Roetzel, W., 2003, "Pool Boiling Characteristics of Nano-fluids," International Journal of Heat and Mass Transfer, **46**(5), pp. 851-862.

[18] Li, C., Akinc, M., Wiench, J., Pruski, M. and Schilling, C.H., 2005, "Relationship between Water mobility and Viscosity of Nanometric Alumina Suspensions," Journal of the American Ceramic Society, **88**(10), pp. 2762-2768.

[19] Heris, S.Z., Etemad, S.G. and Esfahany, M.N., 2006, "Experimental Investigation of Oxide Nanofluids Laminar Flow Convective Heat Transfer," International Communications in Heat and Mass Transfer, **33**(4), pp. 529-535.

[20] Kulkarni, D.P., Das, D.K., and Chukwu, G.A., 2006, "Temperature Dependent Rheological Property of Copper Oxide Nanoparticles Suspension (Nanofluid)," Journal of Nanoscience and Nanotechnology, **6**(4), pp. 1150-1154.

[21] Einstein, A., 1906, "Eine neue Bestimmung der Molekuldimension," Annalen der Physik, **19**, pp. 289-306.

[22] Wen, D.S. and Ding, Y.L., 2004, "Experimental Investigation into Convective Heat Transfer of Nanofluids at Entrance Area under Laminar Flow region," International Journal of Heat and Mass Transfer, **47**(24), pp. 5181–5188.

[23] Xuan, Y.M. and Li, Q., 2003, "Investigation on Convective Heat transfer and Flow features of Nanofluids," ASME Journal of Heat Transfer, **125**, pp. 151–155.

[24] Xie, H., Lee, H., Youn,W. and Choi, M., 2003, "Nanofluids containing Multiwalled Carbon Nanotubes and their Enhanced Thermal Conductivities," Journal of Applied Physics, **94**(8), pp. 4967-4971.

[25] Ohara, T. and Suzuki, D., 2000, "Intermolecular Energy Transfer at a Solid-Liquid Interface," Nanoscale and Microscale Thermophysical Engineering, **4**(3), pp. 189-196.

[26] Jang, S.P. and Choi, S.U.S., 2004, "Role of Brownian Motion in the Enhanced Thermal Conductivity of Nanofluids," Applied Physics Letters, **84**(21), pp. 4316-4318.

[27] Keblinski, P., Phillpot, S. R., Choi, S. U. S., and Eastman, J. A., 2002, "Mechanisms of Heat Flow in Suspensions of Nano-Sized Particles (Nanofluids)," International Journal of Heat and Mass Transfer, **45**(4), 2002, pp. 855–863.

[28] Franks, R., Morefield, S., Jianguo, W., Liao, D., Alvarado, J., Strano, M. and Marsh, C., 2008, "A Study of Nanomaterial Dispersion in Solution by Wet-Cell Transmission Electron Microscopy," Journal of Nanoscience and Nanotechnology, (in print).

[29] Alloush, A., Gosney, W.B. and Wakeham, W.A., 1982, "A Transient Hot Wire Instrument for Thermal Conductivity Measurements in Electrically Conductivity Instruments in Elevated Temperatures," International Journal of Thermophysics, **3**(3), pp. 225-235.

[30] Starr, F.W., Douglas, J.F. and Glotzer, S.C., 2003, "Origin of Particle Clustering in a Simulated Polymer Nanocomposite and its Impact on Rheology," Journal of Chemical Physics, **119**(3), pp. 1777-1788.

[31] Yang, Y., Grulke, E.A., Zhang, Z.G. and Wu, G., 2006, "Thermal and Rheological Properties of Carbon Nanotube-in-Oil Dispersions," Journal of Applied Physics, **99**, pp. 1114307-1-8.

[32] Sohn, C.W. and Chen, M.M., 1981, "Microconvective Thermal Conductivity in Disperse Two Phase Mixture as Observed in a Low Velocity Couette Flow Experiment," Journal of Heat Transfer, Trans. ASME, **103**, pp. 47-51.

[33] Wen, D.S. and Ding, Y.L., 2005, "Effect on Heat Transfer of Particle Migration in Suspensions of Nanoparticles Flowing through Minichannels," Microfluidics and Nanofluidics, **1**(2), pp.183-189.

[34] Kamil, W., 2004, "Heat Transfer in Temperature-dependent Non-Newtonian Flow,"Chemical Engineering and Processing, **43**, pp. 1223-1230.

[35] Kays, W.M. and Crawford, M.E., 1980, *Convective Heat and Mass Transfer*, McGraw-Hill Book Company, New York.

APPENDIX A

SPEED AND SHEAR RATE VALUE

The rotational speed, N (rpm) of the spindle used for viscosity measurements have been converted to corresponding shear rates using Eq. 3.1. The radius of the UL adapter, R_c =1.38 cm and the radius of the spindle used, R_{sp} =1.2575 cm. The values obtained have been tabulated in Table A.1.

Table A.1. Rotational speed and corresponding shear for UL Adapter and Spindle

N, (rpm)	**Shear rate, (sec^{-1})**
10	12.34
12	14.81
20	24.69
30	37.03
50	61.72
60	74.07

APPENDIX B

CALIBRATION OF HEAT TRANSFER SECTION

This section describes the steps undertaken to calibrate the experimental measurements of thermocouples with the theoretical values of temperatures. The thermocouples calibrated include four surface temperature thermocouples ($T_{s,1}$, $T_{s,2,}$ $T_{s,3}$ and $T_{s,4}$) and two bulk temperature thermocouples ($T_{b,i}$ and $T_{b,o}$). The test fluid used for this purpose was de-ionized water. The thermal properties like specific heat, thermal conductivity and viscosity of water were taken at the arithmetic mean of inlet and outlet bulk temperature. These properties were obtained from the National Institute of Standards and Technology (NIST).

The calibration was done both under isothermal conditions without any test fluid and under operating conditions with test fluid.

A.1. Calibration under isothermal conditions

Measurements were taken from each thermocouple in the morning under steady state conditions. The temperature measurements should be same for all the thermocouples after a long period of time. However, due to inherent errors in the accuracy of the thermocouples, it was found that each thermocouple did not give the same value.

Therefore, to make sure that all the thermocouples have a same base value before running the experiments, they were calibrated under isothermal conditions.

Experimental measurements were taken for all the six thermocouples under equilibrium isothermal conditions for a period of 10 days. An arithmetic mean was taken for each thermocouple for 10 days, defined as:

$$T_{average,i} = \frac{\sum_{n=1}^{10} T_{measured,i}}{10} \qquad \text{(B.1)}$$

Where i=1, 2,3,4,5 and 6 is designated to each of the six thermocouples. Based on the above values, a total mean was calculated for each of the average values of the thermocouples, defined as:

$$T_{average,total} = \frac{\sum_{i=1}^{6} T_{average,i}}{6} \qquad \text{(B.2)}$$

Finally, isothermal correction factors (CF_{iso}) were found for each of the corresponding thermocouple based on deviation from the total average, defined as:

$$CF_{iso,i} = T_{average,total} - T_{average,i} \qquad \text{(B.3)}$$

The correction factors thus obtained are shown in Table B.1 and were incorporated directly in the data acquisition system software. It was found that the actual temperature measurement difference ranged between ± 0.1 ^{o}C after this correction factor.

Table B.1. Isothermal correction factors for thermocouples

CF_{iso}					
$T_{s,1}$	$T_{s,2}$	$T_{s,3}$	$T_{s,4}$	$T_{b,i}$	$T_{b,o}$
-0.15	-0.08	0.01	0.10	-0.07	0.19

A.2. Calibration under operating conditions

The experimental set-up was based on the premise that the temperatures at the outside and the inside surfaces of the copper tubing were same due to high thermal conductivity of copper. Therefore, for all practical reasons, the measurements taken by surface mount thermocouples on the outside surface were assumed to be same as the inside temperature. However, due to the limited thermal conductivity of thermally conductive epoxy adhesive used to mount the thermocouples on the copper tubing, the effect of heat from the nichrome wire covering the thermocouple region, and minute geometrical non-conformities in the tubing dimensions, the measured value of temperature was slightly different from the theoretical value. This difference was taken off using the correction factor under operating conditions.

Once, the isothermal correction factors had been applied to each thermocouple, it was compared with the theoretical value of surface temperatures at every location. The steps involved are as follows:

1. The isothermally corrected temperature is defined as :

$$T_{iso,i} = T_{measured,i} + CF_{iso,i} \tag{B.4}$$

2. Based on laminar internally forced flow through a tube of circular cross-section under constant heat flux conditions, values of local Nusselt number for each x/D_i value were found. The method is described in [35] and uses separation of variables and Sturm-Liouville theory to obtain an eigenvalue solution in terms of an infinite series function which gives local Nusselt number as follows:

$$Nu(x) = \left[\frac{1}{Nu_\infty} - \frac{1}{2} \sum \frac{\exp\left(-\gamma_m^2 x^+\right)}{A_m \gamma_m^4} \right]^{-1} \tag{B.5}$$

$$Nu_\infty = 4.364 \tag{B.6}$$

$$x^+ = \frac{2\left(x/D_i\right)}{\mathrm{Re}.\mathrm{Pr}} \tag{B.7}$$

$$\mathrm{Re} = \frac{u.D_i}{\upsilon} \qquad \text{(B.8)}$$

$$\mathrm{Pr} = \frac{\upsilon}{\alpha} \qquad \text{(B.9)}$$

Where $Nu_\infty, D_i, u, \upsilon, \mathrm{Pr}$ and α are fully-developed Nusselt number, inside diameter of copper tubing, mean fluid velocity through test section, kinematic viscosity of the test fluid, Prandtl number, and thermal diffusivity, respectively.

The terms m, γ_m and A_m are defined in Table B.2 as follows:

Table B.2. Infinite series solution for circular tube under constant heat flux conditions. (Adapted : *Convective Heat and Mass Transfer*, Kays and Crawford)

m	γ_m^2	A_m
1	25.68	7.630×10^{-3}
2	83.86	2.058×10^{-3}
3	174.2	0.901×10^{-3}
4	296.5	0.487×10^{-3}
5	450.9	0.297×10^{-3}

3. From the local Nusselt number values found above, corresponding local convective heat transfer coefficient, $h(x)$ were found using Eq. B.10

$$h(x) = \frac{Nu(x).k}{D_i} \qquad \text{(B.10)}$$

Where k is the thermal conductivity of test fluid.

4. The local convective heat transfer coefficient obtained from the above step, was used to find the corresponding surface temperature, $T_s^{'}(x)$ for each of the four surface thermocouples, using Eq. B.11 (same as Eq. 3.7) and heat flux, $q_s^{"}$ from Eq. B.12 (same as Eq. 3.9). It is assumed that the bulk temperature varies linearly from inlet to outlet, and intermediate values were found by linear interpolation.

$$T_s^{'}(x) = \frac{q_s^{"} + \left(h(x).T_b(x)\right)}{h(x)} \qquad \text{(B.11)}$$

$$q_s^{"} = \frac{\dot{m}.c_p(T_{b,o} - T_{b,i})}{A} \qquad \text{(B.12)}$$

5. The values, $T_s^{'}(x)$ or $T_{s,i}^{'}$, where $i = 1, 2, 3$ and 4 obtained from above step were the theoretical surface temperatures obtained in an ideal set-up. These values were then compared with the isothermally corrected values, $T_{iso,i}$ to obtain operating correction factors, $CF_{op,i}$ which is defined as :

$$CF_{op,i} = \frac{T_{s,i}^{'}}{T_{iso,i}} \qquad \text{(B.13)}$$

6. The operating correction factor, $CF_{op,i}$ were found for each surface thermocouple under various flow rates, Q and at constant heat flux, $q_s^{"}$=0.6 W/cm^2. The values obtained are shown in Table B.3.

Table B.3. Operating correction factors under different flow rates.

Flow rate, Q (mL/min)	$CF_{iso,1}$	$CF_{iso,2}$	$CF_{iso,3}$	$CF_{iso,4}$
10	0.92	0.92	0.91	0.91
20	0.95	0.94	0.92	0.91
30	0.95	0.94	0.92	0.91
40	0.95	0.94	0.92	0.90
60	0.95	0.94	0.91	0.89
80	0.95	0.93	0.91	0.89

These results were plotted as shown in Fig. B.1. From the figure, it is seen that after a flow rate of 20 mL/min , the values of the correction factors stabilize significantly as compared to values below 20 mL/min. The standard deviation for the values greater than 20 mL/min was found to be 0.004. This suggested flow rates greater than 20 mL/min in the experiments, and hence, the flow rates of 40 mL/min, 60 mL/min and 80 mL/min.

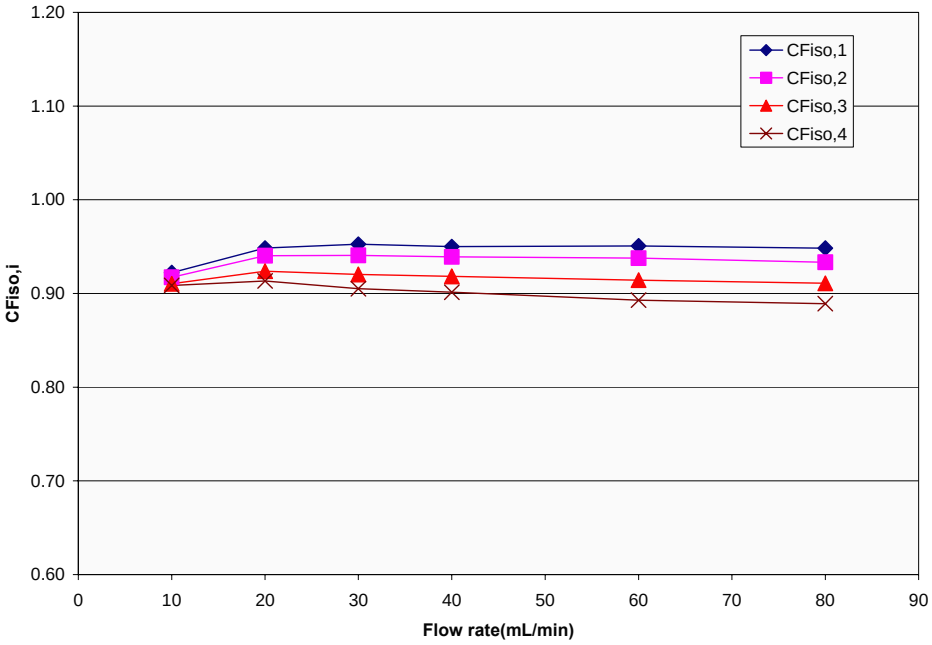

Fig. B.1 Operating correction factors under different flow rates.

7. These operating correction factors are applied to CNT samples as well, using Eq. B.14

$$T_{CNT,s,i} = CF_{op,i}.T_{CNT,iso,i} \qquad \text{(B.14)}$$

Where $T_{CNT,s,i}$ and $T_{CNT,iso,i}$ are the finally corrected surface temperature value and isothermally corrected value obtained directly from data acquisition system (incorporated in hardware), respectively.

APPENDIX C

CALCULATION OF PECLET NUMBER

This section describes the steps undertaken to calculate the Peclet number in the convective heat transfer section, where Peclet number, Pe is defined as:

$$Pe = \frac{\bar{\dot{\gamma}}_f . d_p^2}{\alpha_f} \qquad \text{(C.1)}$$

Where $\bar{\dot{\gamma}}, d_p$ and α_f are local mean shear rate experienced by fluid, particle diameter and thermal diffusivity of the fluid, respectively.

From convective heat transfer fundamentals, in the case of a fully developed laminar flow inside a tube of circular cross section, the velocity can be described as follows:

$$u = U_{\max}\left[1 - \left(\frac{r}{R_i}\right)^2\right] \qquad \text{(C.2)}$$

Where $r = 0$ at the tube centerline, and $r = R_i$ at the tube wall.

Therefore, maximum shear rate, $\dot{\gamma}_w$ can be defined as:

$$\dot{\gamma}_w = \left.\frac{\partial u}{\partial r}\right|_{\max, r=R_i} = -U_{\max}\left(\frac{2}{R_i}\right) = -U_{\max}\left(\frac{4}{D_i}\right) \qquad \text{(C.3)}$$

Additionally,

$$U_{\max} = 2.\overline{U} \qquad \text{(C.4)}$$

$$\overline{U} = \frac{\dot{m}}{A\rho} = \frac{4\dot{Q}}{\pi D_i^2} \qquad \text{(C.5)}$$

Where $U_{\max}, \overline{U}, \dot{m}, A, \rho, \dot{Q}$ and D_i are maximum fluid velocity, mean fluid velocity, mass flow rate, tube inner cross section area, density of fluid, volume flow rate, and inside diameter of tube, respectively.

Using Eq. C.4 and C.5 in C.3, we get

$$\dot{\gamma}_w = \left.\frac{\partial u}{\partial r}\right|_{\max, r=R_i} = \frac{32\dot{Q}}{\pi . D_i^3} \qquad \text{(C.6)}$$

Now, at Re ~ 600 ± 100, $\dot{Q} = 40$ mL/min and $D_i = 1.55$ mm, we get $\dot{\gamma}_w = 1823.5$ sec^{-1} using Eq. C.6.

Also, the local mean shear rate, $\bar{\dot{\gamma}}_f$ could be obtained by:

$$\bar{\dot{\gamma}}_f = \frac{\dot{\gamma}_w}{2} \qquad \text{(C.7)}$$

This gives, $\bar{\dot{\gamma}}_f = 911.75\ \text{sec}^{-1}$

Additionally, thermal diffusivity of the fluid α_f is given by:

$$\alpha_f = \frac{k}{\rho.c_p} \qquad \text{(C.8)}$$

Where k and c_p are the thermal conductivity and specific heat of the fluid, respectively. For MWCNT samples, a typical calculation is done for Sample B (1wt % MWCNT, 40 min sonication) at of 30 °C. The values of ρ and c_p for MWCNT samples was taken same as that of base fluid, DI water as the percentage concentration of MWCNT is small. The values for DI water were taken from NIST at a temperature of 30 °C. However, the thermal conductivity value was taken from the experimental measurements of Sample B at 30 °C.

The values obtained are k = 0.672 W/m.K, $\rho = 995.7\ \text{kg/m}^3$ and $c_p = 4184.1$ kJ/kg.K which gives

α_f =1.61 X 10^{-7} $m^2.sec^{-1}$

Sohn and Chen, 1981 showed that for Pe > 300, significant enhancements were seen in thermal conductivity when solid-liquid dispersion was subjected to shear conditions.

For obtaining suitable thermal conductivity enhancements based on the above phenomenon, Peclet number, Pe should be at least 300. For a Pe = 300, $\bar{\dot{\gamma}}_f$ = 911.75 sec^{-1} and α_f = 1.61 X 10^{-7} $m^2.sec^{-1}$, using Eq. C.1, we obtain a particle diameter, d_p = 230 μm.

VITA

Paritosh Garg was born in Delhi, India. He graduated with first class from Delhi College of Engineering, University of Delhi, India with a Bachelor in Engineering in Mechanical Engineering degree in May 2002. From year, 2002-2006, he worked in engineering and design of power generation, petrochemical and refinery plants. He enrolled at Texas A&M University in the Fall of 2006 and received his Master of Science in Mechanical Engineering in May 2008.

Mr. Garg can be contacted at Flat No. 111, Block-21, Lodhi Colony, New Delhi-110003, India and emailed at paritosh.gg@gmail.com.